Physics – Uspekhi **48** (2) 129 – 149 (2005)

REVIEWS OF TOPICAL PROBLEMS PACS numbers: **71.30.+h**, 73.40.Qv, **73.43.–f**

Metal – insulator transitions and the effects of electron – electron interactions in two-dimensional electron systems

A A Shashkin

DOI: 10.1070/PU2005v048n02ABEH001944

Contents

Abstract. Experimental results on metal – insulator transitions and the anomalous properties of strongly interacting two-dimensional electron systems are reviewed and critically analyzed. Special attention is given to recent results on strongly enhanced spin susceptibility and effective mass in low-disordered silicon MOSFETs.

1. Introduction

Two-dimensional (2D) electron systems are realized when the electrons are free to move in a plane but their motion perpendicular to the plane is quantized in a confining potential well. At low electron densities in such systems, the strongly interacting limit is reached because the kinetic energy is overwhelmed by the energy of electron – electron interactions. The interaction strength is characterized by the ratio $r_s^* = E_{ee}/E_F$ between the Coulomb energy and the Fermi energy. Assuming that the effective electron mass is equal to the band mass, the interaction parameter r_s^* in the single-valley case reduces to the Wigner – Seitz radius $r_s = 1/(\pi n_s)^{1/2} a_B$ and therefore increases as the electron density n_s decreases (here, a_B is the Bohr radius in a semiconductor). Possible candidates for the ground state of the system include Wigner crystal characterized by spatial and spin ordering [1], ferromagnetic Fermi liquid with spontaneous spin ordering [2], paramagnetic Fermi liquid [3], etc. In the strongly interacting limit ($r_s \gg 1$), no analytical theory has been developed to date. According to numeric simulations [4], Wigner crystallization is expected to occur in a very dilute regime, when r_s reaches approximately 35. Refined numeric simulations [5] have predicted that prior to the crystallization, within the range of the interaction parameter $25 \lesssim r_s \lesssim 35$, the ground state of the system is a strongly correlated ferromagnetic Fermi liquid. At higher electron densities, when $r_s \sim 1$, the electron liquid is expected to be paramagnetic, with the effective mass m and Landé g factor renormalized by interactions. Apart from the ferromagnetic Fermi liquid, other intermediate phases between the Wigner crystal and the paramagnetic Fermi liquid may also exist.

In real 2D electron systems, the inherent disorder leads to a drastic change in the above picture, which significantly complicates the problem. According to the scaling theory of localization [6], all electrons in a disordered infinite noninteracting 2D system become localized at zero temperature and zero magnetic field. At finite temperatures, regimes of strong and weak localizations can be distinguished: (i) if the conductivity of the 2D electron layer is activated, the resistivity diverges exponentially as $T \to 0$, and (ii) in the opposite limit of weak localization, the resistivity increases logarithmically with decreasing temperature — an effect originating from the increased probability of electron scattering from impurities back to the starting point. Interestingly, the incorporation of weak interactions ($r_s < 1$) between the electrons promotes the localization [7]. However, for weak disorder and $r_s \gtrsim 1$, a possible metallic ground state was predicted [8 – 10].

In view of the competition between the interactions and disorder, high- and low-disorder limits can be separated. Since many of the experimental groups have made little distinction between these, there has been confusion about interpretation of the data obtained. In highly disordered

A A Shashkin Institute of Solid State Physics,
Russian Academy of Sciences
Chernogolovka, 142432 Moscow Region, Russian Federation
Tel. (7-095) 720-49-59 ext. 2-29 46. Fax (7-096) 524-97-01
E-mail: shashkin@issp.ac.ru

Received 16 June 2004, revised 18 October 2004
Uspekhi Fizicheskikh Nauk **175** (2) 139 – 161 (2005)
Translated by A A Shashkin; edited by A Radzig

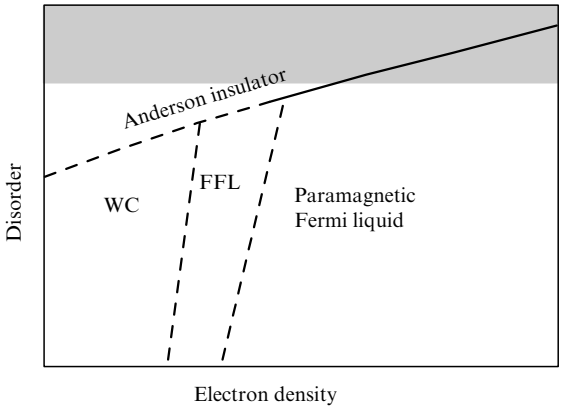

Figure 1. Schematic phase diagram in a disorder-vs-n_s plane. The Wigner crystal (WC) regime is preceded by the ferromagnetic Fermi liquid (FFL) [5]. The high-disorder region is shaded.

electron systems, the range of low densities is unattainable as strong (Anderson) localization sets in (see Fig. 1). At higher electron densities, a logarithmic-in-T correction to the resistivity was observed in numerous experiments (see, e.g., Refs [11 – 13]), providing support for the weak localization theory. Apparently, extrapolation of the weak corrections to $T = 0$ is not justified and, therefore, those studies cannot serve as confirmation of the scaling theory. This theory is remarkable for the principal impossibility of experimental verification because all experiments are performed in samples with finite dimensions at finite temperatures. The question whether or not the scaling theory works is essentially a matter of belief.

The case of low-disordered electron systems is much more interesting. Low electron densities corresponding to the strongly interacting limit become attainable. Experimental results on the metal – insulator phase diagram in perpendicular magnetic fields revealed a close similarity between the insulating phase at low densities and the quantum Hall states. Thus, they exclude the formation of a pinned Wigner crystal in available samples, but support the existence of a metallic state in a zero field [14 – 16]. As the magnetic field is decreased, the extended states in the Landau levels are observed to float up in energy relative to the Landau-level centers and merge to form a metallic state in the $B = 0$ limit. These observations contradict the theoretical scenario according to which in the limit of zero magnetic field the extended states should float up indefinitely in energy [17, 18], thus leading to an insulating ground state. The metallic state was found to be remarkable by the strong drop of resistivity with decreasing temperature [19 – 21]. Although the origin of the phenomenon has been attributed to strong electron – electron interactions, the underlying physics remained unclear until recently.

A breakthrough in understanding this topical problem occurred in the past four years. After a strongly enhanced ratio gm of the spin and cyclotron splittings has been found at low n_s in silicon metal – oxide semiconductor field-effect transistors (MOSFETs) [22], it became clear that the system behaves well beyond the weakly interacting Fermi liquid. It was reported that the magnetic field required to produce complete spin polarization, $B_c \propto n_s/gm$, tends to vanish at a finite electron density $n_\chi \approx 8 \times 10^{10}$ cm^{-2}, which is close to the critical density n_c for the metal – insulator transition in this electron system [23 – 25]. These findings point to a sharp increase in the spin susceptibility $\chi \propto gm$ and possible ferromagnetic instability in dilute silicon MOSFETs. In very dilute GaAs/AlGaAs heterostructures, a similar behavior has been observed in both 2D hole and 2D electron systems [26, 27]. Recently, experimental results have indicated that in silicon MOSFETs it is the effective mass, rather than the g factor, that sharply increases at low electron densities [28]. They have also indicated that the anomalous rise in resistivity with increasing temperature is related to the increased mass. Since the magnitude of the mass does not depend on the degree of spin polarization, this points to a spin-independent origin of the effective mass enhancement [29, 30]. It is interesting to note that the observed phenomena are more pronounced in silicon MOSFETs compared to GaAs/AlGaAs heterostructures, although the fractional quantum Hall effect, which is usually attributed to electron – electron interactions, has not been reliably exposed in silicon MOSFETs.

The fact that n_χ is close to the critical density n_c indicates that the metal – insulator transition in silicon samples with very low disorder potential is a property of a clean 2D system and is driven by interactions [23]. This is qualitatively different from a localization-driven transition in more disordered samples that occurs at appreciably higher densities than n_χ, which in addition are dependent on disorder strength. In this review, attention is focused on the results obtained in the clean regime.

There are several reviews on the topic in question that deserve mention (see, e.g., Refs [31, 32]). However, they have either become outdated or do not express criticism toward items of general belief, for instance, the scaling theory. Below, I describe the main experimental results and draw an overall picture of the metal – insulator transition and anomalous properties of 2D electron systems at low densities.

2. Metal – insulator phase diagrams in a magnetic field

Metal – insulator transitions in perpendicular magnetic fields have attracted a great deal of interest in the past decade. The experimental activity was strongly stimulated by theoretical predictions according to which Wigner crystallization is promoted in the presence of a magnetic field [33 – 37]. Mainly, the insulating phase at low electron densities, whose origin was attributed to possible formation of the Wigner crystal, was studied [38 – 52]. However, this possibility has been precluded in studies of the metal – insulator phase diagram including quantum Hall states, which show a close similarity of all insulating phases in available samples [14 – 16]. It is interesting to note that there are some firmly established experimental results which have not attracted much attention from theorists. These include (i) oscillations of the metal – insulator phase boundary as a function of a perpendicular magnetic field, and (ii) finite bandwidth of extended states in Landau levels.

2.1 Floating-up of extended states in perpendicular magnetic fields

2.1.1 First observation. The scaling theory of localization came into conflict with the quantum Hall effect (quantization of the Hall resistivity $\rho_{xy} = h/\nu e^2$ at integer filling factors ν accompanied with vanishing longitudinal resistivity ρ_{xx}) [53] which implies the existence of extended states in the

Landau levels (see Section 2.3). To reconcile these two, it was theoretically predicted almost immediately that the extended states in the Landau levels cannot disappear discontinuously with decreasing magnetic field but must float up indefinitely in energy in the limit $B \to 0$ [17, 18]. The expected phase diagram is depicted in the inset to Fig. 2a. An equivalent diagram plotted in the disorder versus inverse filling factor ($1/\nu = eB/hcn_s$) plane is known as the global phase diagram for the quantum Hall effect [54]. As long as no merging of the extended states was considered to occur, their piercing of the Fermi level was predicted to cause quantization of the Hall conductivity in weak magnetic fields [55, 56].

The first attempt [14] to experimentally determine the metal–insulator phase diagram in low-disordered silicon MOSFETs at low temperatures has already revealed discrepancies with the theory (see Fig. 2a). In that paper, a somewhat arbitrary criterion for the longitudinal conductivity $\sigma_{xx} = e^2/20h$ was used to map out the phase boundary that corresponds to the Anderson transition to the regime of strong localization. For one thing, however, the phase boundary was shown to be insensitive to the choice of the cutoff value (see, e.g., Ref. [57]); for another, particular cutoff value was consistent with the results obtained for quantum Hall states by vanishing activation energy combined with vanishing nonlinearity of current–voltage characteristics when extrapolated from the insulating phase [15] (note that for the lowest-density phase boundary, a lower value of $\sigma_{xx}^{-1} \approx 100$ kΩ at a temperature of about 25 mK follows from the last-mentioned method). The metallic phase surrounds each insulating phase as characterized by the dimensionless Hall conductivity $\sigma_{xy}h/e^2$ that counts the number of quantum levels below the Fermi level (in bivalley (100)-silicon MOSFETs, spin and valley degeneracies of the Landau level should be taken into account). This indicates that the extended states do not actually disappear discontinuously. Instead, with decreasing magnetic field they float up in energy relative to the Landau-level centers and merge forming a metallic state in the limit $B = 0$ (see Sections 2.2 and 2.4). Besides, the phase boundary at low electron densities oscillates as a function of B with minima corresponding to integer filling factors. The phase boundary oscillations manifest themselves in that at electron densities near the metal–insulator transition at $B = 0$, the magnetoresistance oscillates with an amplitude that diverges as $T \to 0$ [38]; the regions in which the magnetoresistance diverges are referred to as the reentrant insulating phase (see Section 2.2).

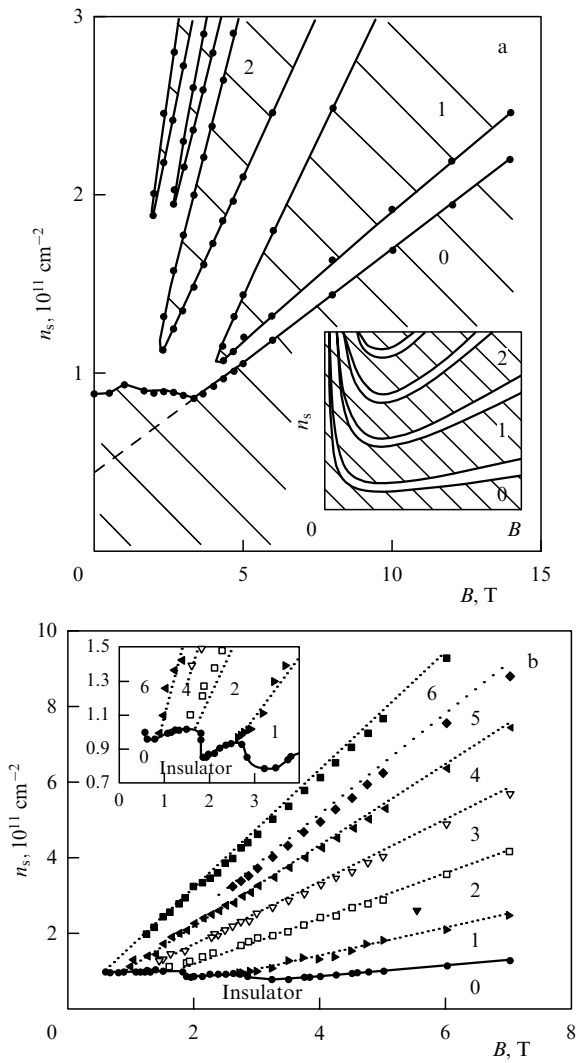

Figure 2. (a) Metal–insulator phase diagram in a low-disordered 2D electron system in silicon MOSFETs, obtained using a cutoff criterion $\sigma_{xx} = e^2/20h$ at a temperature of $T \approx 25$ mK. The dimensionless Hall conductivity $\sigma_{xy}h/e^2$ in different insulating phases is indicated. The slope of the dashed line is close to $e/2hc$. A sketch of the expected phase diagram is displayed in the inset. (Taken from Ref. [14].) (b) Map of extended states determined by maxima in σ_{xx} in a low-disordered silicon MOSFET. Numbers designate σ_{xy} in units of e^2/h. (Adopted from Ref. [58].)

2.1.2 Other methods and 2D carrier systems. The topology of the observed metal–insulator phase diagram, i.e., merging the extended states and, hence, the presence of direct transitions between the insulating phase with $\sigma_{xy} = 0$ and quantum Hall phases with $\sigma_{xy}h/e^2 > 1$, is robust, being insensitive to the method for spotting the phase boundary [15, 58] and to the choice of 2D carrier system [59, 60]. It was verified using a criterion of vanishing activation energy and vanishing nonlinearity of current–voltage characteristics as extrapolated from the insulating phase, which allows more accurate determination of the Anderson transition [15]. Kravchenko et al. [58] also applied a method that had been suggested in Ref. [61] for similar silicon MOSFETs. They studied extended states by tracing maxima in the longitudinal conductivity in the (B, n_s)-plane (see Fig. 2b) and found good agreement with the aforementioned results. A similar merging of at least the two lowest extended states was observed in more disordered 2D hole systems in a GaAs/AlGaAs heterostructure [59] (see Fig. 3a) and in a Ge/SiGe quantum well [60] (see Fig. 3b). In the former case, the extended states were determined by peaks in σ_{xx} or temperature-independent crossing points in ρ_{xx}; in the latter, they were associated either with maxima in ρ_{xx} and/or $d\rho_{xy}/dB$, or with crossing points of ρ_{xx} at various temperatures. It is noteworthy that a bad combination of the criterion for determining the phase boundary and the 2D carrier system under study may lead to a failure when mapping out the phase diagram down to relatively weak magnetic fields. In Ref. [61], extended states were studied by measuring maxima in the longitudinal conductivity in the (B, n_s)-plane for the strongly disordered 2D electron system in GaAs/AlGaAs heterostructures (see Fig. 3c). Because of strong damping of the Shubnikov–de Haas oscillations in weak magnetic fields, the desired region in the phase diagram below 2 T was not reached in that experiment. This invalidates the claim by Glozman et al. [61] that the extended states do not merge [62]. The behavior

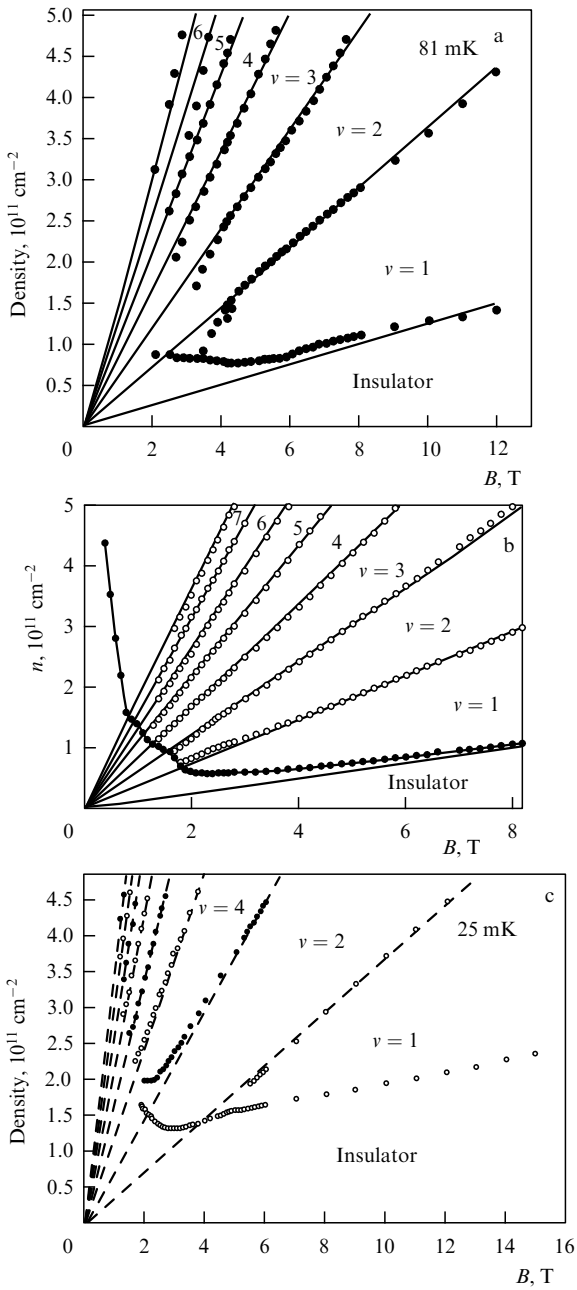

Figure 3. (a) Map of the extended states for a highly disordered 2D hole system in GaAs/AlGaAs heterostructures. Each data point represents a distinct peak in σ_{xx} or a temperature-independent crossing point in ρ_{xx}. Numbers show the value of $\sigma_{xy}h/e^2$. (Adopted from Ref. [59].) (b) Map of the extended states for a highly disordered 2D hole system in a Ge/SiGe quantum well. The open circles represent maxima in ρ_{xx} and/or $\mathrm{d}\rho_{xy}/\mathrm{d}B$. The full circles correspond to crossing points of ρ_{xx} at different temperatures. Numbers show the value of $\sigma_{xy}h/e^2$. (Adopted from Ref. [60].) (c) Behavior of the extended states determined by maxima in σ_{xx} in a strongly disordered 2D electron system in GaAs/AlGaAs heterostructures. Numbers designate σ_{xy} in units of e^2/h. (Adopted from Ref. [61].)

of the lowest extended state in Fig. 3c, which in the view of Glozman et al. [61] floats up above the Fermi level as $B \to 0$, simply reflects the occurrence of a phase-boundary oscillation minimum at the filling factor $\nu = 2$, similar both to the minimum at $\nu = 1$ in Fig. 3a and to the case of silicon MOSFETs (see Fig. 2). Such a minimum manifests itself in that there exists a minimum in ρ_{xx} for integer $\nu \geqslant 1$ that is straddled by the insulating phase [38, 63 – 67]. To this end, all available data for the metal – insulator phase diagrams agree well with each other, except those in the vicinity of $B = 0$. In weak magnetic fields, experimental results obtained in 2D electron systems with high disorder are not method-independent. Glozman et al. [61] found that the cutoff criterion yields basically a flat phase boundary down to $B = 0$, which is in agreement with the data for silicon MOSFETs (Fig. 2a). On the contrary, Hilke et al. [60] employed the method based on temperature dependences of ρ_{xx} and obtained a turn-up at the phase boundary in Fig. 3b. Note that the validity of the data in Fig. 3b for the lowest extended state in magnetic fields $\lesssim 1.5$ T is questionable because the weak temperature dependences of ρ_{xx} as analyzed by Hilke et al. [60] cannot be related trustworthily to either an insulator or a metal. The same applies to similar temperature dependences observed, for instance, in Refs [68 – 74].

2.1.3 Weak-field regime. As a matter of fact, the weak-field problem — whether or not there is an indefinite rise in the phase boundary as $B \to 0$ — reduces to a problem of the existence of a metal – insulator transition at $B = 0$ and $T = 0$. In diluted 2D electron systems with low enough disorder, the resistivity ρ strongly drops with lowering temperature, providing an independent way of facing the issue. Given strong temperature dependences of ρ, those with $\mathrm{d}\rho/\mathrm{d}T > 0$ ($\mathrm{d}\rho/\mathrm{d}T < 0$) can be associated with a metallic (insulating) phase [19 – 21, 75, 76]. If extrapolation of the temperature dependences of ρ to $T = 0$ is tolerable, the curve with $\mathrm{d}\rho/\mathrm{d}T = 0$ should correspond to the metal – insulator transition. The fact that this method and the one based on vanishing activation energy combined with vanishing nonlinearity of current – voltage curves when extrapolated from the insulating phase give equivalent results strongly supports the existence of a true metal – insulator transition in a zero magnetic field [77] (see also Section 2.4). As long as in more-disordered 2D carrier systems the metallic behavior ($\mathrm{d}\rho/\mathrm{d}T > 0$) is suppressed (see, e.g., Refs [78 – 85]) or disappears entirely, it is definitely incorrect to extrapolate those weak temperature dependences of ρ to $T = 0$ with the aim of distinguishing between insulator and metal. Once one of the two methods fails, it remains to be seen how to verify the conclusion as inferred from the other method. This makes uncertain the existence of a true metal – insulator transition at $B = 0$ in 2D electron systems with high disorder.

2.1.4 Phase boundary oscillations. The next important point is the oscillating behavior of the phase boundary that restricts the insulating phase with $\sigma_{xy} = 0$ (see, for instance, Fig. 2). It is worth noting that the oscillations persist down to the magnetic fields corresponding to the fillings of higher Landau levels, as indicated also by magnetoresistance oscillations [38, 63, 67]. The oscillation period includes the following elements. With decreasing magnetic field, the lowest extended states follow the Landau level, then float up in energy relative to its center, and finally merge with extended states in the next quantum level. The last stage was absent in the original considerations [17,18, 54, 55], thus leading to discrepancies between experiment and theory. Recently, theoretical efforts have been concentrated on modifications of the global phase diagram for the quantum Hall effect to reach topological compatibility with the observed metal – insulator phase diagram. It has been predicted that the spin-up and spin-down extended states in the Landau level should merge [86, 87] (see Fig. 4a). However, as

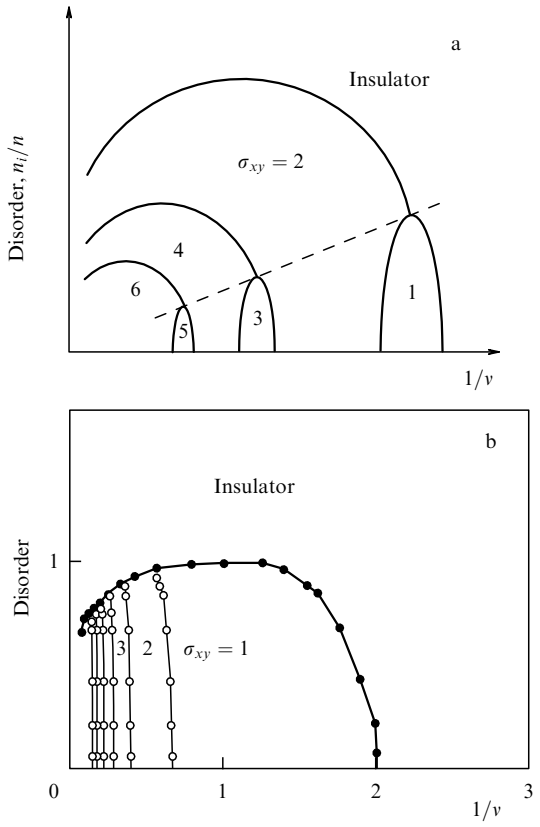

Figure 4. (a) Sketch of the modified global phase diagram for the quantum Hall effect as expected from the mean-field approximation neglecting the Zeeman energy. The dashed line corresponds to the collapse of the exchange-enhanced spin splitting. (Adopted from Ref. [86].) (b) Numerical results for the phase diagram within a tight-binding model. (Adopted from Ref. [103].)

regards lowest extended states, the topology of the phase diagram changes for the lowest Landau level only; moreover, they do not float up before merging. It has been verified that shifts of the extended states from the Landau-level centers that are caused by disorder-induced mixing of the Landau levels are small [88–93]. Within tight-binding models, an indication had been first obtained that the extended states disappear [94–96], which caused some criticism of the relevance of such a lattice model to the continuum system [97, 98]. After that, a floating up of the extended states without merging has been found in studies [99–101]. On the contrary, Sheng and Weng [102, 103] have found a merging of the extended states, although without an oscillating behavior of the lowest extended state (see Fig. 4b). As for now, the effect of the phase boundary oscillations is still far from being fully described theoretically.

Concluding this section, I would like to make a couple of remarks on alternative ways for determining the metal–insulator phase boundary. An attempt was made to spot the phase boundary in the limit $B = 0$ using the $\sigma_{xy} = e^2/2h$ criterion [104]. However, this particular value of σ_{xy} has no special meaning as $B \to 0$. An idea was put forth to relate the minimum in the inverse compressibility to the metal–insulator transition [105]. However, it has been recently shown that this minimum lies at carrier densities well above the critical density for the percolation metal–insulator transition in a zero magnetic field [106]. Particularly, in highly disordered 2D carrier systems, its position may be close to that of the crossing point of the resistivity curves at various temperatures [105], which formally yields overestimated densities for the metal–insulator transition because of suppression of the metallic behavior (see Section 2.4).

2.2 Similarity of the insulating phase and quantum Hall phases

2.2.1 Method for comparison and consequences. About a decade ago, attention was mainly paid to the insulating phase at low electron densities as a possible candidate for the Wigner crystal. It was argued that its aforementioned reentrant behavior was a consequence of the competition between the quantum Hall effect and the pinned Wigner crystal [38, 39]. Another certain argument was the strongly nonlinear current–voltage characteristics in the insulating phase, which were attributed to depinning of the Wigner crystal [40, 41]. Similar properties of the insulating phase in 2D electron (near $\nu = 1/5$) [42–49] and 2D hole (near $\nu = 1/3$) [50–52] systems in GaAs/AlGaAs heterostructures with relatively low disorder were also attributed to a pinned Wigner crystal which is interrupted by the fractional quantum Hall state. An alternative scenario was discussed in terms of percolation metal–insulator transition [57, 107, 108]. To distinguish between the two scenarios, the behavior of activation energy and current–voltage characteristics in the insulating phase was studied and compared to that in quantum Hall phases [15, 16, 109].

In contrast to the low-density insulating phase, the way for determining the current–voltage characteristics of the quantum Hall phases is different for Corbino and Hall bar geometries. In the former, the dissipationless Hall current does not contribute to the dissipative current that is proportional to σ_{xx}, thus allowing straightforward measurements of current–voltage curves for all insulating phases. In the latter, the two current channels are connected through edge channels (see Section 2.3), and current–voltage characteristics correspond to quantum-Hall-effect breakdown curves. The dissipative backscattering current I that flows between opposite edge channels is balanced by the Hall current across the filled Landau levels and associated with the longitudinal voltage V_{xx}. As long as $\sigma_{xx} \ll \sigma_{xy}$, the quantized value of σ_{xy} is a factor that allows the determination of $I = \sigma_{xy} V_{xx}$ and the Hall voltage $V = I_{\rm sd}/\sigma_{xy}$ from the experimental breakdown dependence of V_{xx} on source–drain current $I_{\rm sd}$. The dependence $V(I)$ constitutes a current–voltage characteristic, which is equivalent to the case of Corbino geometry [15] (see Fig. 5). Not only are the current–voltage curves similar for all insulating phases, but they behave identically near the metal–insulator phase boundaries (see Fig. 6a). The dependence of the critical voltage $V_{\rm c}$ on the distance from the phase boundary is close to a parabolic law [41, 57]. The phase boundary position determined by a vanishing $V_{\rm c}$ is practically coincident with that determined by a vanishing activation energy $E_{\rm a}$ of electrons from the Fermi level $E_{\rm F}$ to the mobility edge $E_{\rm c}$ (see Fig. 6b). The value of E_a is determined from the temperature dependence of the conduction in the linear interval of current–voltage curves, which is activated at not too low temperatures [110]; notice that it transforms into variable range hopping when $T \to 0$ (see below). The activation energy changes linearly with the distance from the phase boundary, reflecting the constancy of the thermodynamic density of states near the transition point (see also Section 2.4). The threshold behavior of the current–voltage

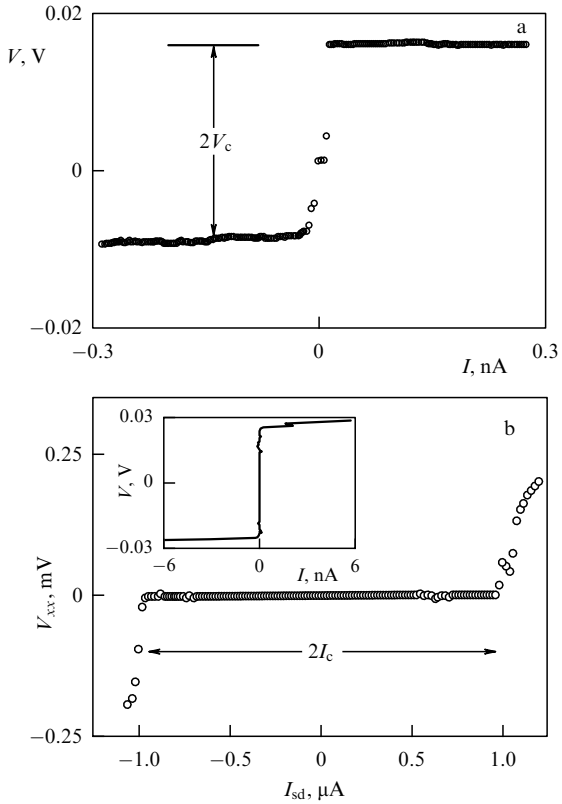

Figure 5. Current – voltage characteristics in a low-disordered silicon MOSFET in $B = 12$ T at $T \approx 25$ mK for (a) the low-density insulating phase at $n_s = 1.74 \times 10^{11}$ cm^{-2}, and (b) the insulating phase with $\sigma_{xy}h/e^2 = 1$ at $n_s = 2.83 \times 10^{11}$ cm^{-2}. In figure (b), the measured breakdown dependence $V_{xx}(I_{sd})$ was converted into current – voltage characteristics (inset). (Taken from Ref. [15].)

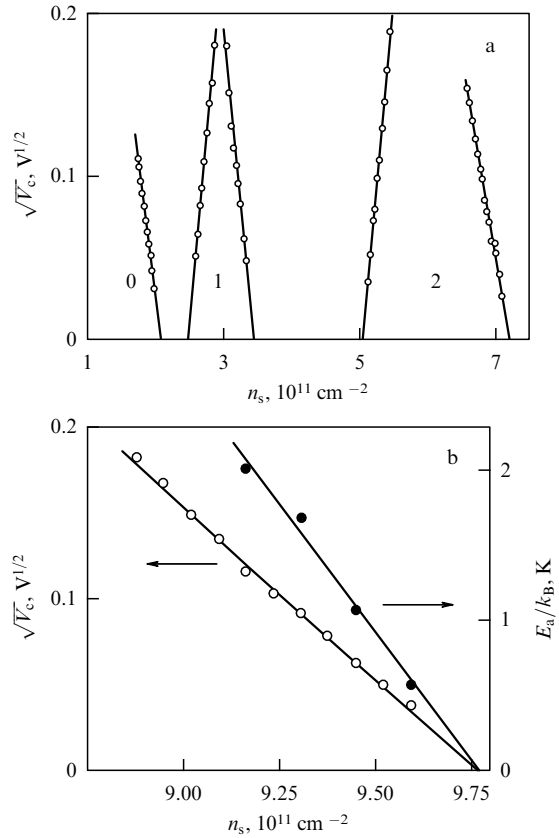

Figure 6. (a) Square root of the critical voltage as a function of electron density at the phase boundaries corresponding to $\sigma_{xy}h/e^2 = 0$, 1, and 2 in the field of $B = 12$ T for a low-disordered 2D electron system in silicon MOSFETs. (b) Behavior of the critical voltage and the activation energy near the phase boundary in $B = 16$ T. (Taken from Ref. [15].)

characteristics is caused by the breakdown in the insulating phases. The breakdown occurs when the localized electrons residing at the Fermi level gain enough energy to reach the mobility threshold in an electric field V_c/d over a distance given by the localization length L [15, 111]:

$$\frac{eV_cL}{d} = |E_c - E_F|\,, \tag{1}$$

where d is the corresponding sample dimension. The quantities E_a and V_c are related through the localization length which is temperature-independent and diverges near the transition as $L(E_F) \propto |E_c - E_F|^{-s}$ with the exponent s close to unity, in agreement with the theoretical value $s = 4/3$ in the classical percolation problem [112]. The values of the localization length are practically the same near all metal – insulator phase boundaries, which indicates that even quantitatively all insulating phases are very similar. Note that since the localization length in Eqn (1) is small compared to the sample dimensions, the phase boundary position determined by the diverging localization length refers to an infinite 2D system. As inferred from the vanishing of both E_a and V_c at the same point (see Fig. 6b), possible shifts in the mobility threshold due to finite sample dimensions are small, which in turn justifies extrapolations to the limit of $L \to \infty$.

The consequences of the above-considered method include:

(i) insofar as no dramatic changes in transport properties occur, this excludes the pinned Wigner solid as the origin for the insulating phase at low electron densities in the available samples of low-disordered silicon MOSFETs;

(ii) the metal – insulator phase diagram in Fig. 2a is verified and substantiated;

(iii) the existence of a metal – insulator transition in zero magnetic field is supported (see Section 2.4), and

(iv) the bandwidth of the extended states in the Landau levels is finite.

All of these are also valid for relatively low-disordered 2D carrier systems in GaAs/AlGaAs heterostructures with the distinction that fractional quantum Hall phases are involved. Nevertheless, the topology of the phase diagram remains unchanged, including the oscillating behavior of the phase boundary that restricts the low-density insulating phase (see Fig. 7). Additional confirmation of the percolation transition to the low-density insulating phase in GaAs/AlGaAs heterostructures was received by studying the high-frequency conductivity [113] and time-resolved photoluminescence of 2D electrons [114], as discussed in Ref. [16].

2.2.2 Finite bandwidth of extended states. It was predicted two decades ago that the localization length diverges as a power law at a single energy E^* falling in the center of the Landau level: $L(E) \propto |E - E^*|^{-s}$ [115 – 117]. The idea to check this prediction based on low-temperature measurements of σ_{xx} [118] was quickly developed to a concept of single-parameter scaling [119]. It was suggested that the magnetoresistance tensor components are functions of a single variable defined

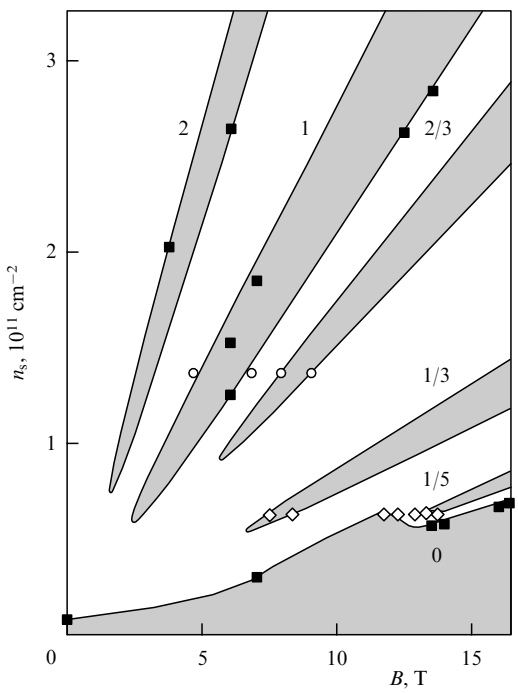

Figure 7. Metal–insulator phase diagram in a relatively low-disordered 2D electron system in GaAs/AlGaAs heterostructures. The points corresponding to phase boundaries were obtained (1) in two samples using the criteria of vanishing activation energy and vanishing nonlinearity of current–voltage curves as extrapolated from the insulating phase (circles and squares), and (2) on one sample from Ref. [113] using a cutoff criterion $\sigma_{xx}^{-1} = 10$ MΩ at a temperature of $T \approx 25$ mK as follows from the former method (diamonds). The solid lines display guides for the eye. The numbers indicate values of $\sigma_{xy}h/e^2$ for different insulating phases. (Taken from Ref. [16].)

as the ratio between the dephasing length $L_d(T) \propto T^{-p/2}$ (where p is the inelastic-scattering-time exponent) and the localization length. The concept was claimed to be confirmed by measuring the temperature dependences of the peak width ΔB in ρ_{xx} (or σ_{xx}) and the maximum of $d\rho_{xy}/dB$ in a highly disordered 2D electron system in InGaAs/InP heterostructures, the measurements which yielded $\Delta B \propto T^{\varkappa}$, where $\varkappa = p/2s \approx 0.4$ [120]. Later on, both deviations in the power law and different exponents in the range between $\varkappa = 0.15$ and $\varkappa = 1$ were observed for other 2D carrier systems, different Landau levels, and various disorder strengths [65, 68, 69, 121–140]. Importantly, the scaling analysis of the experimental data in question is based on two unverified assumptions: (i) zero bandwidth of the extended states in the Landau levels, and (ii) constancy of the thermodynamic density of states in the scaling range. If either assumption is invalid, this may lead at least to underestimating the experimental value of the exponent $\varkappa$.

The method based on vanishing activation energy and vanishing nonlinearity of current–voltage characteristics as extrapolated from the insulating phase shows that the former assumption is not justified. Moreover, measurements of the ρ_{xx} peak width as a function of temperature in low-disordered silicon MOSFETs yield a linear dependence which extrapolates to a finite peak width as $T \to 0$, according to Ref. [15] (see Fig. 8). Very similar temperature (and frequency) dependences were observed in highly disordered 2D carrier systems in GaAs/AlGaAs heterostructures [141, 142] and Ge/SiGe heterostructures [66, 143]. It is noteworthy that a

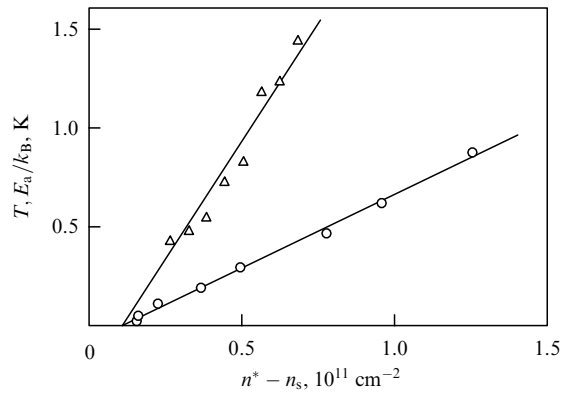

Figure 8. Temperature dependence of the ρ_{xx} peak width ($n^* - n_s$) at half-height of the peak counted from the density n^* corresponding to $\nu^* = 2.5$ (circles), and the behavior of the activation energy (triangles) in a low-disordered silicon MOSFET in the field $B = 14$ T. (Taken from Ref. [15].)

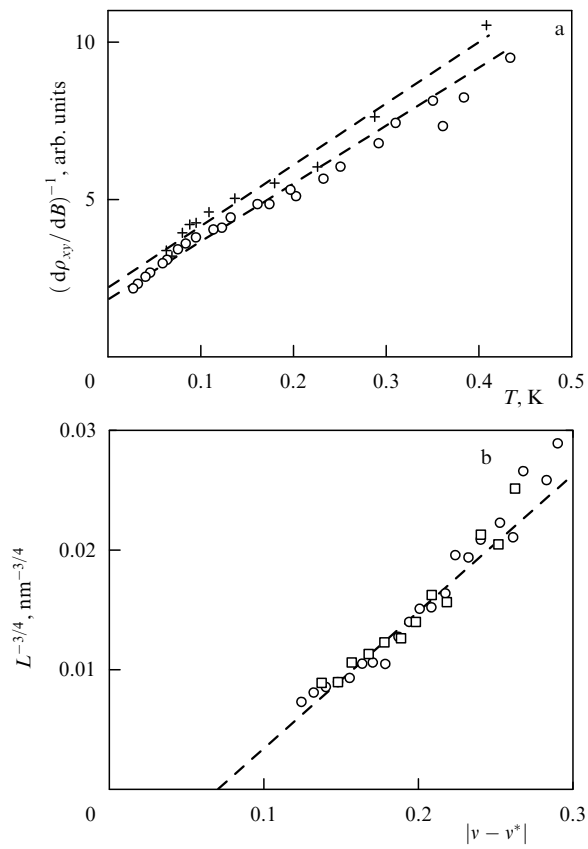

Figure 9. (a) Temperature dependence of the ρ_{xx} peak width as determined from the maximum of $d\rho_{xy}/dB$ at $\nu^* = 1.5$ in a highly disordered 2D electron system in GaAs/AlGaAs heterostructures. Distinct symbols correspond to different runs. The dashed lines are linear fits to the data. (Adopted from Ref. [126].) (b) Localization length determined by the high-frequency conductivity in the variable-range-hopping regime in a highly disordered 2D electron system in GaAs/AlGaAs heterostructures as a function of the filling factor deviation from $\nu^* = 2.5$ (squares) and $\nu^* = 3.5$ (circles) towards the $\nu = 3$ plateau. The dashed line is a linear fit expected from the classical percolation approach with the exponent $s = 4/3$. (Adopted from Ref. [138].)

similar behavior is revealed if the data from the publications which claim the observation of scaling are plotted on a linear rather than logarithmic scale (see, e.g., Fig. 9); finite values of the peak width as $T \to 0$ are even more conspicuous for the

data of Refs [123 – 125]. The reason for the ambiguity is quite simple: within the limits of experimental error, it is difficult (on a logarithmic scale it is especially difficult) to distinguish between sublinear/superlinear fits to the data and linear fits which do not necessarily run to the origin.

Although lack of data in most of the above-cited experimental papers does not allow one to verify the validity of both assumptions, it is very likely that there is no qualitative difference between all of the discussed results. As a matter of fact, they can be described by a linear (or weakly sublinear) temperature dependence with a finite offset at $T = 0$. Here is an alternative and simple explanation of the temperature dependence of the ρ_{xx} peak width in terms of thermal broadening. Within a percolation picture, if the activation energy $E_a \sim k_B T$, the conduction is on the order of the σ_{xx} maximum, so that the value of $\sim k_B T$ provides a thermal shift to the effective mobility edge corresponding to the σ_{xx} peak width [15]. Despite the fact that the concept of thermal broadening has been basically ignored in the literature in search for not so trivial data interpretations, it looks as if no experimental results go beyond this favoring of the concept of single-parameter scaling. Once the behavior of the localization length is not reflected by the temperature-dependent peak width in ρ_{xx}, no experimental support is provided for numeric calculations of the localization length, which give a somewhat larger exponent $s \approx 2$ compared to $s = 4/3$ in the classical percolation problem (see, e.g., Ref. [144]). The latter value of s, as well as the behavior of the localization length in Fig. 6, have been recently confirmed by measurements of the high-frequency conductivity in the variable-range-hopping regime [138] (see Fig. 9b).

Thus, the finding of finite bandwidth of the extended states in the Landau levels [15, 16], which is in obvious contradiction to scaling arguments, is a firmly established experimental result. Astonishingly, it has had no theoretical interpretation for ten years.

2.2.3 The Hall insulator. Deep in the interior of insulating phases and at low temperatures, the variable-range-hopping regime occurs in which the conductivity σ_{xx} is small compared to its peak value [112]. In this regime, it was predicted that the deviation $\Delta\sigma_{xy}$ of the conductivity σ_{xy} from its quantized value in strong magnetic fields is much smaller than $\sigma_{xx} \propto \exp\left[-(T_0/T)^{1/2}\right]$ [145]: $\Delta\sigma_{xy} \propto \sigma_{xx}^{\gamma}$ with the exponent $\gamma \approx 1.5$; notice that this is in contrast to a straightforward linear relationship in the activation regime, as inferred from approximately the same behavior of the ρ_{xx} peak width and the maximum of $\mathrm{d}\rho_{xy}/\mathrm{d}B$ with a change in temperature. Later on, finite ρ_{xy} contrasted with diverging ρ_{xx} was found in calculating the magnetotransport coefficients at $T = 0$ in the insulating phase with vanishing σ_{xx} and σ_{xy} [146, 147]. Such a behavior of ρ_{xx} and ρ_{xy} indicates a special quadratic relation between conductivities:

$$\sigma_{xy} \propto \sigma_{xx}^2 \,. \tag{2}$$

Moreover, it was shown that ρ_{xy} is close to the classical value $(B/n_s ec)$ [148], providing arguments for the existence of a Hall insulator phase [54].

Values of ρ_{xy} close to $B/n_s ec$ were experimentally found in the low-density insulating phase, deviations from the classical Hall line being attributed to a possible admixture of ρ_{xx} [43, 63, 149 – 154]. Thus, the distinction of the Hall insulator phase from the quantum Hall phases — that is, the absence of extended states below the Fermi level — becomes evident when expressed in terms of ρ_{xx} and ρ_{xy}.

It was empirically found in low-disordered silicon MOSFETs that the lowest-filling-factor peak in σ_{xx} plotted in the $(\sigma_{xy}, \sigma_{xx})$-plane is close to a semicircle centered at $(e^2/2h, 0)$ [39, 108, 154]. The semicircle law for the lowest-ν peak was reproduced in a highly disordered 2D hole system in a Ge/SiGe quantum well [72, 73]. It was shown in these works that the semicircle relation originates directly from conductivity/resistivity tensor inversion:

$$\sigma_{xx}^2 + \left(\sigma_{xy} - \frac{e^2}{2h}\right)^2 = \left(\frac{e^2}{2h}\right)^2 + \frac{1 - \rho_{xy} e^2/h}{\rho_{xx}^2 + \rho_{xy}^2} \,, \tag{3}$$

because the (narrow) σ_{xx} peak in question is located at a filling factor just below $\nu = 1$ (see, for instance, Fig. 2) where ρ_{xy} is still close to h/e^2. Although this finding is consistent with available theories [155 – 159], the semicircle law does not seem universal if higher-ν peaks in σ_{xx} with different heights are involved [39, 123, 154, 160].

2.3 Edge channel effects and direct measurements of the quantized Hall conductivity

In a magnetically quantized 2D electron system, the Landau levels bend up at the sample edges due to the confining potential, and edge channels form where these levels intersect the Fermi energy (see, e.g., Ref. [161]). The natural question arises whether the current in the quantum Hall state flows in the bulk or at the edges of the sample. Although the Hall conductivity σ_{xy} was not directly measured in early experiments on the quantum Hall effect, it seemed obvious that this quantity corresponds to ρ_{xy}, in agreement with the concept of currents that flow in the bulk [162]; it is a matter of course that finite σ_{xy} would give evidence for the existence of extended states in the Landau levels [155, 161]. This concept was challenged by the edge current model [163]. In this approach, extended states in the bulk of a sample are not crucial and the problem of current distributions in the quantum Hall effect is reduced to a one-dimensional task in terms of transmission and reflection coefficients as determined by the backscattering current at the Fermi level between the sample edges. Importantly, if the edge current contributes significantly to the total current, conductivity/resistivity tensor inversion is not justified because the conductivities σ_{xx} and σ_{xy} are related to the bulk of the 2D electron system.

To verify whether or not the Hall conductivity is quantized, direct measurements of σ_{xy} were necessary for excluding a possible shunting effect of the edge currents. Being equivalent to Laughlin's gedanken experiment [164, 165], such measurements were realized using the sample of Corbino geometry which allows separation of the bulk contribution to the total current [166 – 173]. A Hall charge transfer below the Fermi level between the boundaries of a Corbino sample is induced by magnetic field sweep through the generated azimuthal electric field. If $\sigma_{xx} \to 0$, no discharge occurs allowing determination of the transferred charge

$$Q = \sigma_{xy} \pi r_{\mathrm{eff}}^2 c^{-1} \delta B \,, \tag{4}$$

where r_{eff} is the effective radius. The induced voltage $V = Q/C$, which is restricted due to a large shunting capacitance C, changes linearly with the magnetic field, with

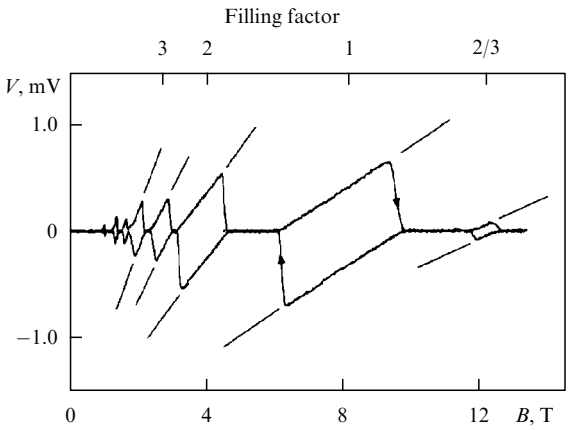

Figure 10. The induced voltage in a Corbino sample of a GaAs/AlGaAs heterostructure in up- and down-sweeps of the magnetic field. Also shown by straight lines are the expected slopes for $\nu = 2/3$, 1, 2, 3, and 4. (Taken from Ref. [168].)

a slope determined by σ_{xy} in the quantum Hall states until the dissipationless quantum Hall state breaks down (see Fig. 10). The fact that the quantization accuracy of σ_{xy} (about 1%) is worse compared to that of ρ_{xy} may be attributed to the nonconstancy of the effective area in moderately homogeneous samples. Thus, the Hall current in the quantum Hall effect flows not only at the edges but also in the bulk of the 2D electron system through the extended states in the filled Landau levels.

Apparently, the dissipative backscattering current in Hall bar samples should be balanced by Hall current through the filled Landau levels, thus resulting in a longitudinal potential drop [174]. This point makes a significant contribution to the edge current model.

From an experimental viewpoint, all edge channel effects proceed from slow equilibration (over macroscopic distances) between the electrochemical potentials of different edge states, including the state in the bulk of a sample. As long as such an equilibration occurs on the edges at the Fermi level, the applicability of the edge state model is justified. The approach accounts for the phenomena observed in conventional transport experiments, which include nonlocal resistance and effects related to contacts/reservoirs (see, e.g., Ref. [175]). However, particular potential profiles at the edge and current distributions can be probed only using nondestructive spatially resolved imaging techniques [176–194]; notice that many of the so-revealed inhomogeneous samples show quite good magnetotransport characteristics. Contrary to standard considerations of the edge channels in terms of skipping orbits for a confining potential that sharply changes over the magnetic length $l_B = (\hbar c/eB)^{1/2}$, it turned out that in most samples the potential profile at the edge is smooth and spans much larger distances than l_B. Edge regions corresponding to approximately 10-μm scale of a confining potential were visualized in Hall photovoltage optical imaging experiments on standard Hall bar samples [183] (see Fig. 11a). Since the Hall electric field is nearly constant, even if some field enhancement occurs near the edges [176], the edge current contribution can be appreciable depending on the particular sample.

For a soft confining potential, edge channels are also referred to as compressible and incompressible strips whose spacing is determined by the electron density gradient [195]. This is very similar to the long-standing phenomenon of Hall current pinch: given electron density gradients, the Hall current basically flows through narrow channels (or incompressible strips) determined by the minimal σ_{xx}, their position in the sample being controlled, for instance, by a magnetic field [181, 182, 196–199]. When located at the edge, the pinch of Hall current becomes identical with the subject broached in Ref. [195]. The Hall current channels at the edge of a sample were imaged using a single-electron transistor as a probe for the local σ_{xx} [184] (see Fig. 11b). Applying a negative voltage to a side gate leads to a shift in the edge of the 2D electron system towards the probe, thereby creating a line scan of the local σ_{xx} across the sample edge. Vanishing σ_{xx} is indicated by enhanced fluctuations in the feedback signal, the feedback circuit being used to keep the current through the single-electron transistor constant by controlling its voltage relative to the 2D electron system.

With respect to the preceding subsections, the insignificance of edge channel effects in transport experiments is verified in the usual way by coincidence of the results obtained in Hall bar and Corbino geometries.

2.4 True zero-field metal–insulator transition and phase boundary in parallel magnetic fields

As has been discussed above, the existence of extended states in quantizing magnetic fields was established by two independent experimental methods: (i) quantization of σ_{xy}, and (ii) vanishing activation energy and vanishing nonlinearity of current–voltage characteristics as extrapolated from the insulating phase. Theory is generally in agreement with this evidence, even though there are unresolved problems with finite bandwidth of the extended states in the Landau levels. In contrast, no extended states are expected in a zero magnetic field, at least for weakly interacting 2D electron systems. The second experimental criterion, however, leads to the opposite conclusion, although it does not have absolute credibility alone. To sort it out, further support by independent experimental verifications is needed.

Alternative criterion is based on analysis of the temperature dependences of the resistivity in the field $B = 0$. Provided they are strongly varied, those with positive (negative) derivative $\mathrm{d}\rho/\mathrm{d}T$ are indicative of a metal (insulator) [19–21, 75, 76]; note that in the vicinity of the transition, $\rho(T)$ dependences obey the scaling law with the exponent $\varkappa \approx 1$, which is consistent with the concept of thermal broadening/shift by the quantity $\sim k_{\mathrm{B}}T$ of the effective mobility edge in the insulating phase (see Section 2.2). If extrapolation of $\rho(T)$ to $T = 0$ is valid, the critical point for the metal–insulator transition is given by $\mathrm{d}\rho/\mathrm{d}T = 0$. In a low-disordered 2D electron system in silicon MOSFETs, the resistivity at a certain electron density shows virtually no temperature dependence over a wide range of temperatures [200–202] (see Fig. 12a). This curve separates those with positive and negative derivative $\mathrm{d}\rho/\mathrm{d}T$ nearly symmetrically at temperatures above 0.2 K [203]. Assuming that it remains flat down to $T = 0$, one can obtain the critical point n_{c} which corresponds to a resistivity $\rho \approx 3h/e^2$ [31].

Recently, these two criteria have been applied simultaneously to the 2D metal–insulator transition in low-disordered silicon MOSFETs [77, 202]. In a zero magnetic field, both methods yield the same critical density (see Figs 12b and 13b). Since one of them is temperature-independent, this equivalence strongly supports the existence

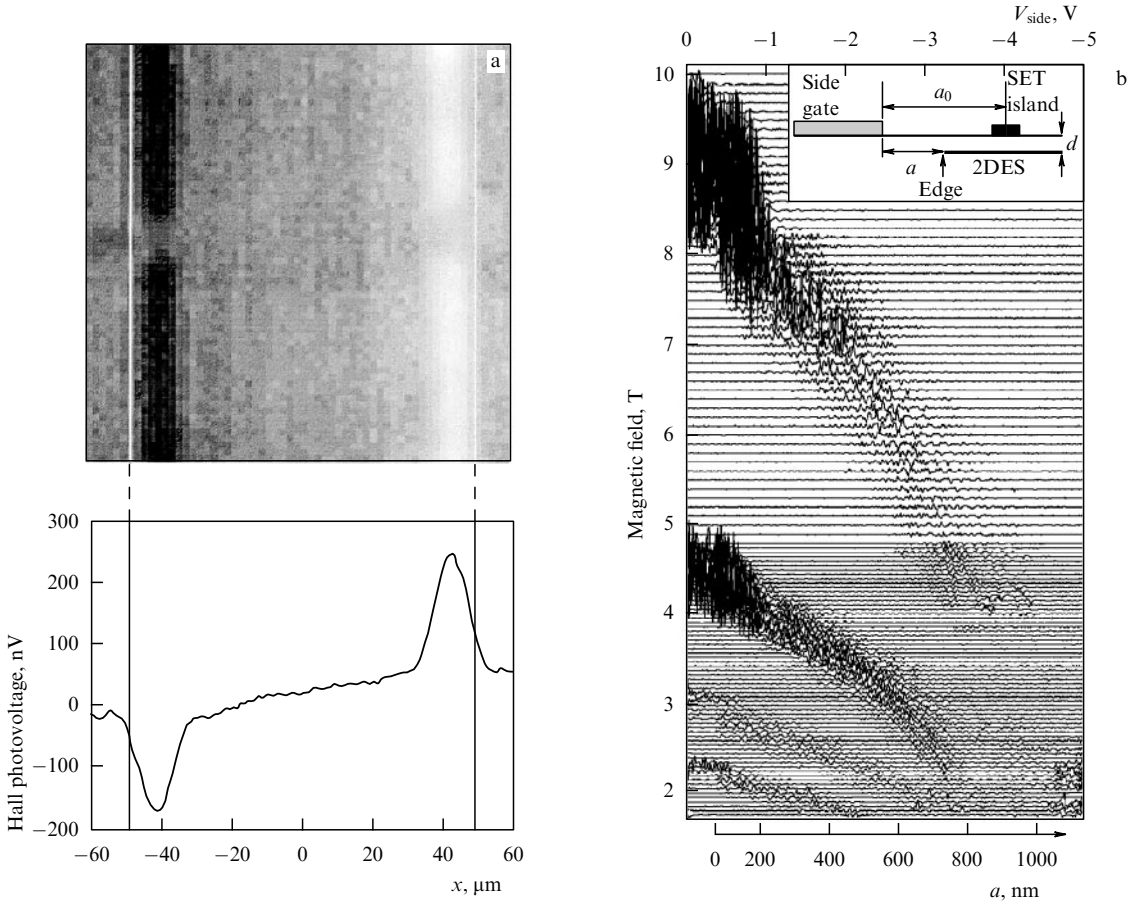

Figure 11. (a) Image of Hall photovoltage in a near-surface GaAs/AlGaAs heterojunction at $\nu = 2$ (top) and a line scan taken horizontally through the image (bottom). The spot size is 5 μm across. The physical edges of the sample are indicated by vertical lines. (Taken from Ref. [183].) (b) Traces of the fluctuation part of the feedback signal vs. the side-gate voltage V_{side} for shifting the edge in a GaAs/AlGaAs heterostructure in different magnetic fields. Enhanced fluctuations in the feedback signal indicate vanishing σ_{xx}, which corresponds to Hall current channels (incompressible strips) for $\nu = 1, 2, 3$, and 4. (Adopted from Ref. [184].)

of a true metal – insulator transition at $B = 0$. This also bolsters confidence that the curve with the zero derivative $d\rho/dT$ will remain flat (or at least will retain finite resistivity value) down to zero temperature. Additional confirmation in favor of a true zero-field metal – insulator transition is provided by magnetic measurements as described in the next section.

In the presence of a parallel magnetic field $B_{\parallel}$, the outcome is very different. With increasing parallel field, the transition point $n_c(B_{\parallel})$ determined from the vanishing nonlinearity and activation energy shifts approximately linearly to higher electron densities, being saturated above a critical field $B_c \approx 3$ T at a constant value which is approximately 1.5 times higher than that in a zero magnetic field. Note that a similar suppression of the metallic state was observed using a cutoff criterion $\rho = 100$ kΩ [108]. In the metallic phase, the saturation of the resistance with a parallel magnetic field testifies to the onset of full spin polarization of the 2D electrons, as inferred from an analysis of Shubnikov – de Haas oscillations in tilted magnetic fields [204 – 206]. One might expect that the 2D electron system is spin-polarized for parallel fields $B_{\parallel} > B_c$, and that the observed phase boundary shift exhibits a spin effect. At the so-determined critical density $n_c(B_{\parallel})$, the exponential divergence of the resistivity as $T \to 0$ dies out, although $d\rho/dT$ remains negative at least for $B_{\parallel} > B_c$ (see Figs 12c and 13b). In a magnetic field, contrary to the zero-field case, not only are the $\rho(T)$ curves asymmetric about the middle curve in Fig. 12c, but all of them have negative derivatives $d\rho/dT$ in the entire temperature range, although the values of ρ are comparable to those in the $B = 0$ case. The metallic ($d\rho/dT > 0$) temperature dependence of the resistivity, observed at higher electron densities in parallel magnetic fields, is weak, so that the derivative method does not yield a critical density for $B_{\parallel} > B_c$. Its failure leaves uncertain the existence of a true metal – insulator transition in a parallel magnetic field.

A very similar conclusion holds for 2D electron systems with higher disorder in a zero magnetic field (see Section 2.1). In this case, the metallic ($d\rho/dT > 0$) behavior is also suppressed [78 – 85] or disappears entirely, and extrapolation of the weak $\rho(T)$ dependences to the limit $T = 0$ is not justified, invalidating the derivative criterion for determining the critical point of the metal – insulator transition (see Fig. 13c). It is noteworthy that, owing to its simplicity, the derivative method is widely used when describing metallic ($d\rho/dT > 0$) and insulating ($d\rho/dT < 0$) temperature dependences of resistivity in a restricted temperature range. To avoid confusion with metallic and insulating phases, however, one should employ alternative methods for determining the metal – insulator transition point. Such methods, including a vanishing activation energy and noise measurements, have been applied to highly disordered 2D carrier systems

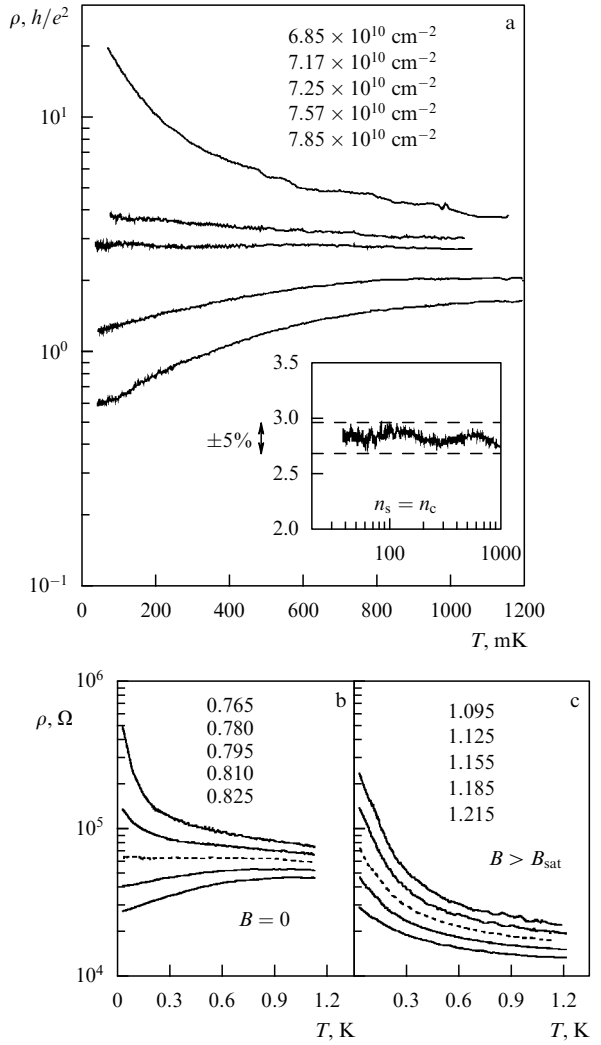

Figure 12. (a) Resistivity as a function of temperature at different electron densities in a low-disordered silicon MOSFET. The inset shows the middle curve on an expanded scale. (Adopted from Ref. [201].) (b, c) Temperature dependence of the resistivity of a low-disordered silicon MOSFET at different electron densities near the metal–insulator transition in a zero magnetic field (b), and in a parallel magnetic field of 4 T (c). The electron densities are indicated in units of 10^{11} cm^{-2}. (Taken from Ref. [77].)

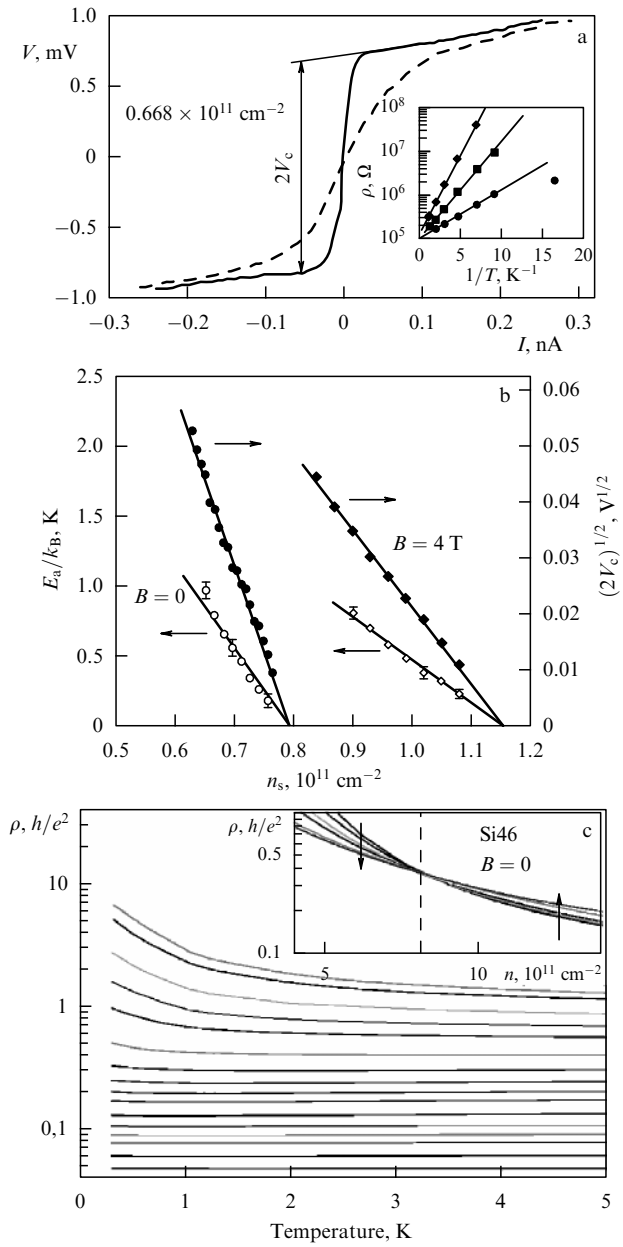

Figure 13. (a) Current–voltage characteristics in a zero magnetic field at $T \approx 30$ mK (solid line) and 211 mK (dashed line) for the same silicon MOSFET as in Figs12b, c; note that the threshold voltage is practically independent of temperature. An Arrhenius plot of the resistivity in the insulating phase is displayed in the inset for different values of $B_{\parallel}$ and n_s. (Taken from Ref. [77].) (b) Activation energy and square root of the threshold voltage as functions of electron density in a zero magnetic field (circles) and in a parallel magnetic field of 4 T (diamonds). The critical densities correspond to the dashed lines in Figs 12b, c. (Taken from Ref. [77].) (c) Resistivity versus temperature in a strongly disordered silicon MOSFET at the following electron densities: 3.85, 4.13, 4.83, 5.53, 6.23, 7.63, 9.03, 10.4, 11.8, 13.2, 16.0, 18.8, 21.6, 24.4, 30.0, and 37.0×10^{11}cm^{-2}. The $\rho(n_s)$ isotherms are given in the inset. (Adopted from Ref. [85].)

[202, 207, 208]. Being similar, they yield lower critical densities for the metal–insulator transition, compared to those obtained formally using the derivative criterion. This simply reflects the fact that the metallic ($\mathrm{d}\rho/\mathrm{d}T > 0$) behavior of the resistivity is suppressed, the critical density n_c increasing naturally with disorder strength (see Fig. 1).

3. Many-body phenomena in diluted 2D electron systems

The resistivity drop with decreasing temperature in a low-disordered 2D electron system in silicon MOSFETs in a zero magnetic field turned out to be stronger compared to the metallic $\rho(T)$ expected from the temperature-dependent screening theories [209–212] and was attributed to a manifestation of strong electron–electron interactions [19]. Recently, the underlying physics of the effect has been clarified. A greatly enhanced ratio gm between the spin and the cyclotron splittings has been found at low electron densities, thus indicating that the 2D system behaves well beyond the weakly interacting Fermi liquid [22]. Experimental results have also shown that it is the effective mass that sharply increases at low electron densities and is related to the anomalous rise in the resistivity with temperature [28]. In view of quantum phase transitions at $T = 0$, while for the

insulating phase a transition is signaled by the diverging localization length, the interaction-enhanced mass may be a similar indicator for the metallic phase.

3.1 Increase in the product *gm* near the metal – insulator transition and possible ferromagnetic transition

3.1.1 Beating pattern of Shubnikov – de Haas oscillations. Electron – electron interactions give rise to a renormalization of the Fermi-liquid parameters, including the effective mass and g factor [3]. Tracing Shubnikov – de Haas oscillation minima in a 2D electron system in tilted magnetic fields, it is easy to determine the ratio gm between spin and cyclotron splittings, which is proportional to the spin susceptibility χ. In the range of high electron densities $n \geqslant 2 \times 10^{11}$ cm^{-2} in silicon MOSFETs, moderate enhancements of gm by a factor of $\leqslant 2.5$ were observed [204, 213, 214], which is consistent with the concept of a weakly interacting Fermi liquid.

At low electron densities in low-disordered silicon MOSFETs placed in perpendicular magnetic fields, the Shubnikov – de Haas oscillation minima corresponding to the cyclotron splittings ($\nu = 4, 8, 12, 16, \ldots$) were found to disappear as the electron density is reduced [22] (see Fig. 14). Disregarding the minimum for the valley splitting at $\nu = 1$, only minima corresponding to the spin splittings ($\nu = 2, 6, 10, 14, \ldots$) remain close to the metal – insulator transition which occurs in the samples studied at $n_c \approx 8 \times 10^{10}$ cm^{-2}. These results disclose that as one approaches the metal – insulator transition, the cyclotron gaps (which are equal to the difference between the cyclotron and spin splittings, ignoring the valley splitting) become smaller than the spin gaps and eventually vanish. The condition for vanishing is an equality of the spin and the cyclotron splittings, or $gm/2m_e = 1$ (where m_e is the free electron mass) which is higher by more than a factor of 5 than the value of this ratio in bulk silicon: $gm/2m_e = 0.19$. The phenomenon cannot be explained in the framework of the many-body enhancement of spin gaps in a perpendicular magnetic field [215 – 219] because the disappearance of the cyclotron gaps over a wide range of magnetic field intensities would require an enhanced g factor which is independent of the magnetic field. This implies that the product gm is nearly field-independent and approximately equal to its enhanced many-body zero-field value (see Section 3.2). Thus, the spin susceptibility $\chi \propto gm$ is greatly enhanced near the metal – insulator transition.

Similar experiments in tilted magnetic fields cannot provide high accuracy in determining the behavior of the renormalized gm at low electron densities because there are

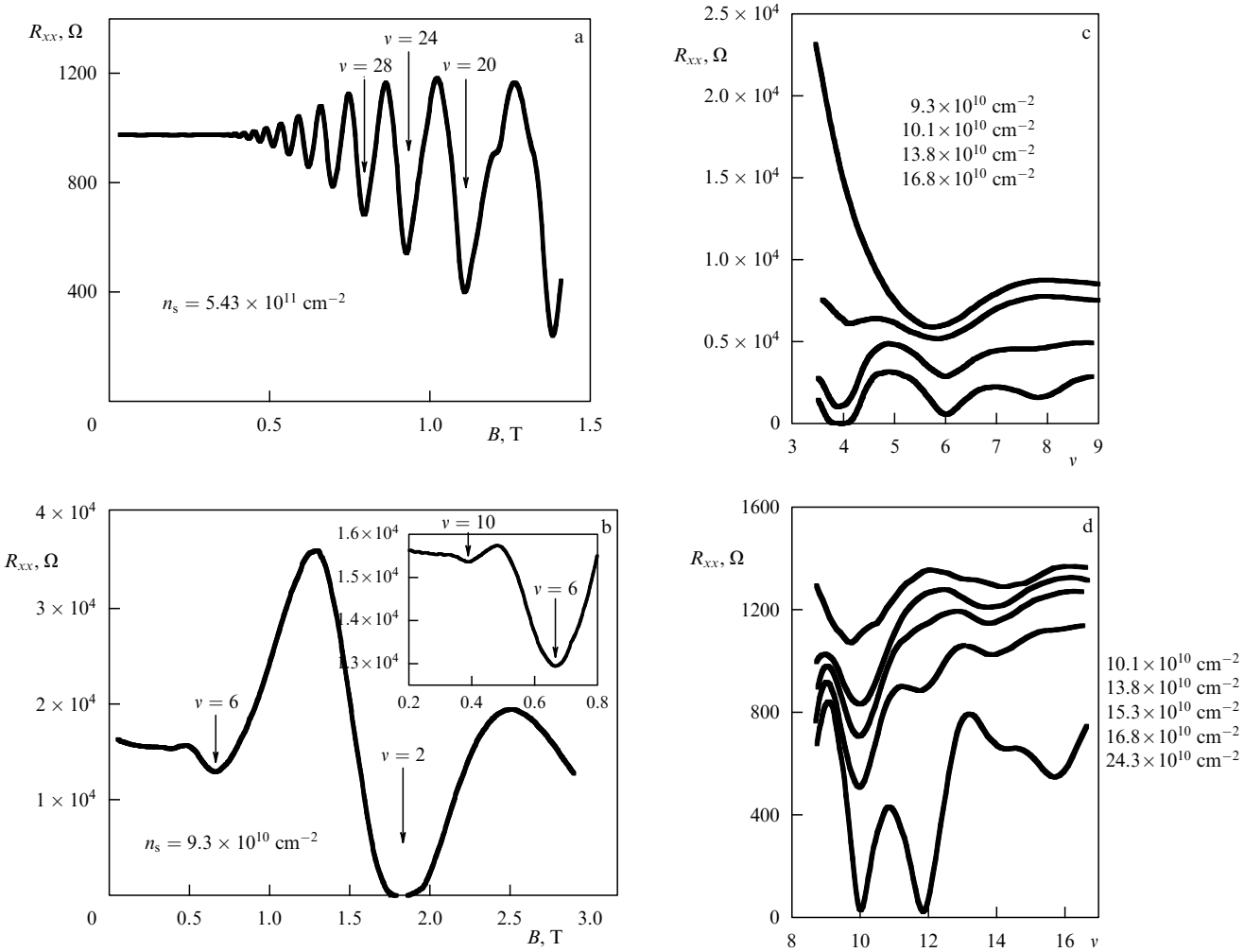

Figure 14. Shubnikov – de Haas oscillations in a low-disordered silicon MOSFET at a temperature of $T \approx 40$ mK for high (a) and low (b) electron densities. (c, d) Evolution of the Shubnikov – de Haas oscillations with the electron density n in two ranges of filling factors. The curves at various n are arbitrarily shifted along the y-axis for clarity. (Taken from Ref. [22].)

too few Shubnikov–de Haas oscillations near the metal–insulator transition. Nevertheless, high enough accuracy was attained in experiments on the parallel-field magnetotransport.

3.1.2 Scaling the parallel-field magnetoresistance and other procedures. As the thickness of the 2D electron system in silicon MOSFETs is small compared to the magnetic length in accessible fields, the parallel magnetic field couples largely to the electrons' spins, while the orbital effects are suppressed. The resistance in dilute silicon MOSFETs was found to be isotropic with respect to the in-plane magnetic field and rise steeply with the field, tending to saturation at a constant value above a critical field B_c which depends on the electron density [220–222] (see Fig. 15a). As has been mentioned in Section 2.4, the saturation field B_c corresponds to the onset of full spin polarization of the electron system [204–206].

It was found in a low-disordered 2D electron system in silicon MOSFETs that the normalized magnetoresistivity measured at different electron densities in the low-temperature limit in which $\rho(B_\parallel)$ becomes temperature-independent collapses onto a single curve when plotted as a function of $B_\parallel/B_c$, where the scaling parameter B_c is normalized to correspond to the saturation/polarization field [23] (see Figs 15b, c). The scaling breaks down when one approaches the metal–insulator transition where the magnetoresistivity strongly depends on temperature even at the lowest experimentally achievable temperatures. Note that the observed scaling dependence is described reasonably well by the theoretical dependence of $\rho/\rho(0)$ on the degree of spin polarization, $\xi = gm\mu_B B_\parallel/\pi\hbar^2 n_s = B_\parallel/B_c$, which arises due to the spin-polarization-dependent screening of a random potential [223]. The field B_c is proportional, with a high degree of precision, to the deviation in the electron density from its critical value: $B_c \propto (n_s - n_c)$ (see Fig. 16a). The procedure used provides high accuracy for determining the functional form of $B_c(n_s)$, even though the absolute value of B_c is determined not so accurately. Since the considerable increase in the product gm at low electron densities (see Fig. 16b), which follows from the $B_c(n_s)$ dependence, is in agreement with the enhanced gm obtained from Shubnikov–de Haas oscillations, the band tail of localized electron states is small and the clean limit shows up. Therefore, the tendency for B_c to vanish at a finite electron density n_χ close to n_c gives evidence in favor of the existence of a ferromagnetic transition in this electron system, thus indicating that the metal–insulator transition is driven by interactions [23]. It signifies that the vicinity of either tricritical point is reached in the phase diagram of Fig. 1 (see Section 3.3).

A similar conclusion about possible spontaneous spin polarization was drawn based on a scaling of magnetoconductivity data in similar samples at different electron densities and temperatures [24]. Results for the greatly enhanced gm were corroborated in detailed studies of Shubnikov–de Haas oscillations in dilute silicon MOSFETs with higher disorder in tilted magnetic fields [224] (see Fig. 16c). The agreement among all three sets of data is remarkable, especially if one takes into account that different teams used different experimental procedures, dissimilar samples, and various field/spin-polarization ranges [25]. This also indicates that the electron density $n_\chi \approx 8 \times 10^{10}$ cm^{-2} is sample-independent, in contrast to the critical density n_c for the metal–insulator transition. Obviously, for the spin susceptibility $\chi \propto gm$ to diverge at $n_s = n_\chi$, the extrapolation of $B_c(n_s)$ to

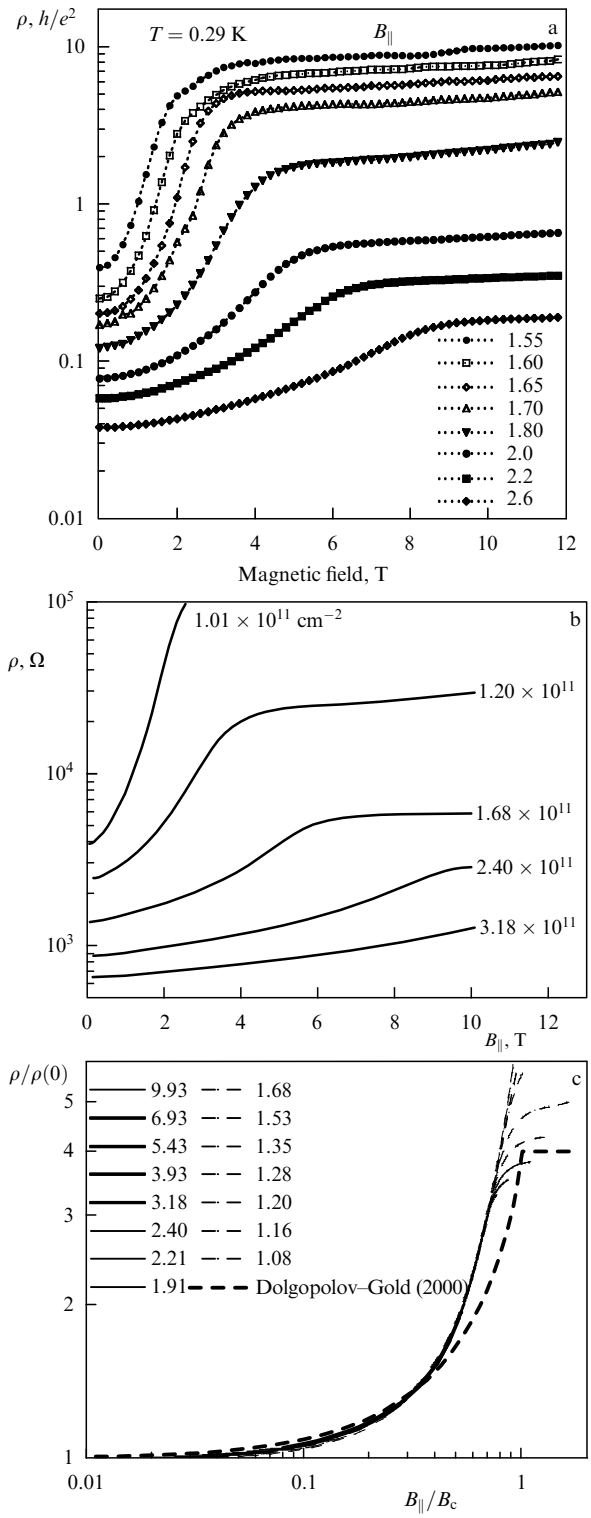

Figure 15. (a) Resistivity versus parallel magnetic field, measured on a low-disordered silicon MOSFET. Different symbols correspond to gate voltages from 1.55 to 2.6 V, or to electron densities from 1.01 to 2.17×10^{11} cm^{-2}. (Adopted from Ref. [221].) (b) Low-temperature magnetoresistivity of a low-disordered 2D electron system in silicon MOSFETs in parallel magnetic fields at different electron densities above n_c for the metal–insulator transition at $B = 0$. (Taken from Ref. [23].) (c) Scaled curves of the normalized magnetoresistivity vs. $B_\parallel/B_c$. The electron densities are indicated in units of 10^{11} cm^{-2}. Also shown by a dashed line is the normalized magnetoresistivity calculated by Dolgopolov and Gold [223]. (Taken from Ref. [23].)

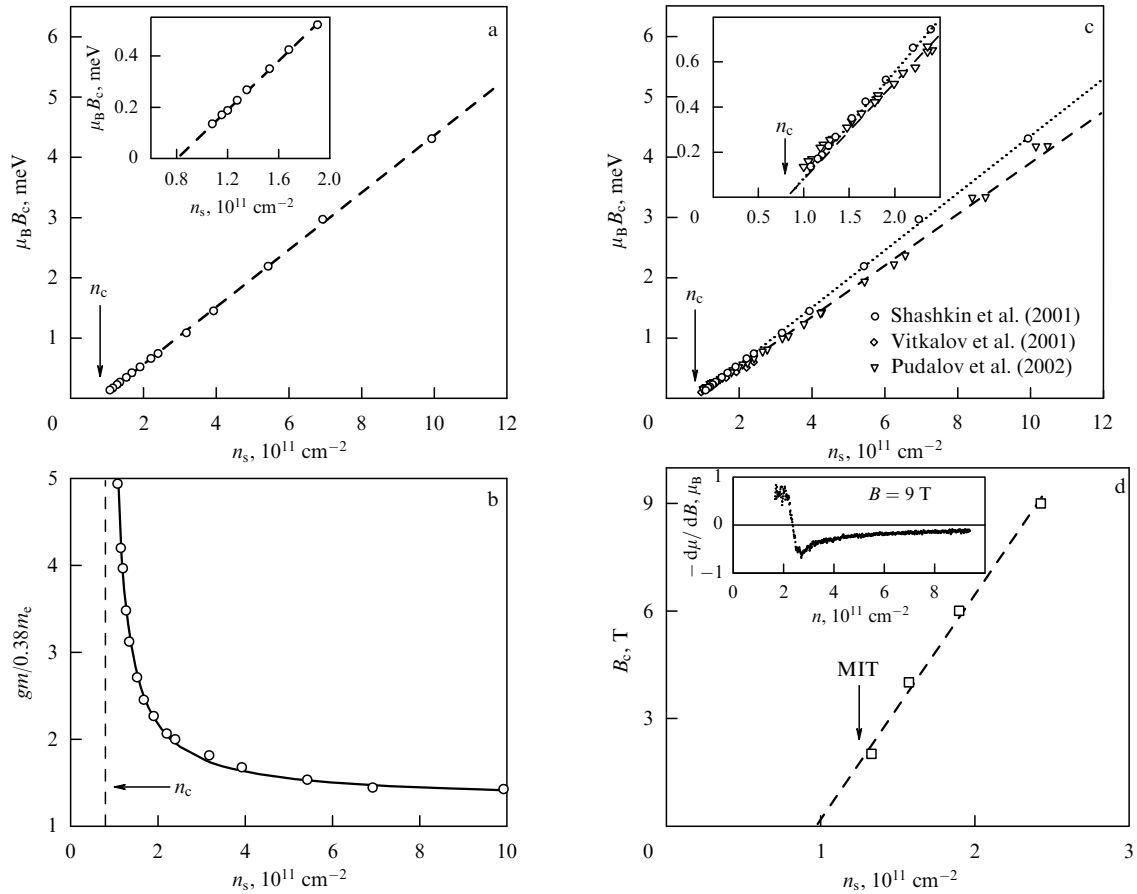

Figure 16. (a) Dependence of the field B_c on electron density in a low-disordered silicon MOSFET. The dashed line is a linear fit. (Taken from Ref. [23].) (b) The product gm versus electron density, obtained from the data for B_c. (Taken from Ref. [23].) (c) Polarization field as a function of electron density obtained by different groups [23, 24, 224]. The critical density n_c in the samples from Ref. [23] is indicated. (Taken from Ref. [25].) (d) Polarization field vs. electron density in a highly disordered silicon MOSFET, as determined from $d\mu/dB_{\|} = 0$ at 0.2 K. The dashed line is a linear fit. The evaluated position of the metal – insulator transition is indicated. The derivative $d\mu/dB_{\|}$ as a function of electron density in a parallel magnetic field of 9 T at a temperature of 100 mK is displayed in the inset. (Adopted from Ref. [227].)

zero must be valid. To verify its validity, accurate data at lower densities, lower temperatures, and on much less disordered samples are needed [25, 225, 226].

Thermodynamic investigations of the spin susceptibility, based on measurements of the chemical potential change with parallel magnetic field, $d\mu/dB_{\|}$, were performed in highly disordered silicon MOSFETs, as inferred from the considerably higher densities for the metal – insulator transition [227] (see Fig. 16d, cf. Fig. 16c). As compared to the clean regime, the obtained dependence of the polarization field B_c on n_s in Fig. 16d is shifted to appreciably higher electron densities owing to local moments in the band tail [222, 227 – 229]. The band tail effects thus become crucial in parallel field experiments on highly disordered 2D electron systems.

3.1.3 Other 2D carrier systems. A similar enhancement of the spin susceptibility at low electron densities was found in dilute GaAs/AlGaAs heterostructures through the analysis of the Shubnikov – de Haas oscillations [27] (see Fig. 17a). The thickness of the 2D carrier system in GaAs/AlGaAs heterostructures is relatively large, which leads to an increase in the effective mass with a parallel magnetic field [27, 230 – 234]. As a result, the magnitude of the polarization field, obtained from the parallel-field magnetoresistance, becomes strongly reduced as the electron density increases. Disregarding this reduction, both data sets allow determination of the $B_c(n_s)$ dependence whose critical behavior is not so evident, possibly because the lowest experimentally reached densities are still too high. Due to the lower effective mass, the higher dielectric constant, and the absence of valley degeneracy, the same interaction strength $r_s^* = E_{ee}/E_F$ in the 2D electron system in GaAs/AlGaAs heterostructures is likely to be achieved at densities about two orders of magnitude lower than in silicon MOSFETs. Therefore, the existence of a critical region is expected for electron densities $n_s < 10^9$ cm^{-2} which have not yet been accessed in currently available samples of GaAs/AlGaAs heterostructures.

The orbital effects in parallel magnetic fields can be avoided by using narrow quantum wells. A 2D electron system in narrow AlAs quantum wells is similar to that in silicon MOSFETs, except that the valley degeneracy is absent in the former [235]. The critical region expected for densities $n_s < 2 \times 10^{10}$ cm^{-2} is well exceeded by the lowest attainable electron densities in narrow AlAs quantum wells with high disorder (see Fig. 17b). Note that the data points relating to the insulating phase reflect the physics of local moments in the band tail [222, 227 – 229], which is different from that in the metallic phase.

Being very similar to silicon MOSFETs, a 2D electron system in Si/SiGe quantum wells differs by the higher

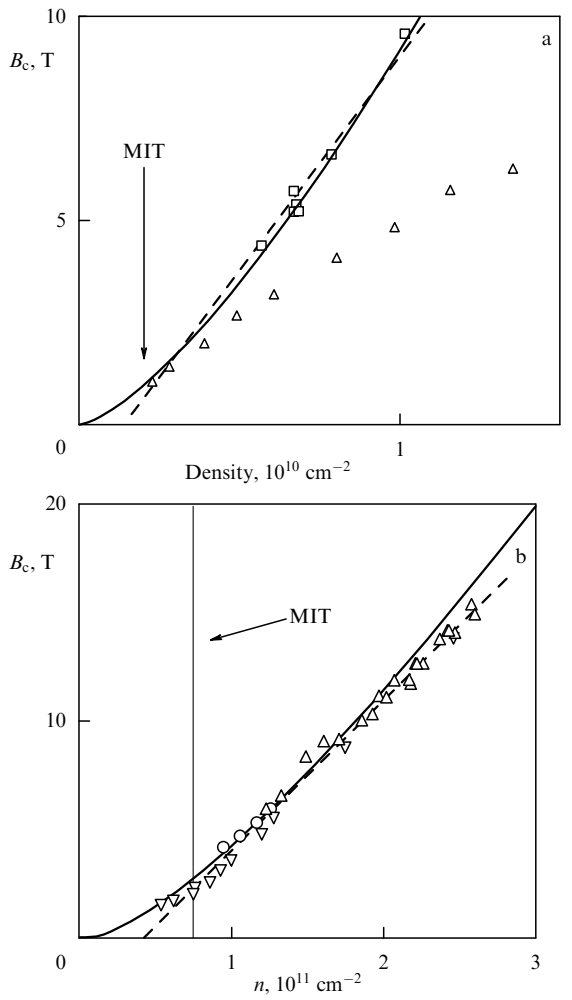

Figure 17. (a) Data for B_c as a function of electron density in a dilute GaAs/AlGaAs heterostructure, obtained by Shubnikov – de Haas oscillations (squares) and parallel-field magnetoresistance (triangles). The power-law fit $B_c \propto n_s^{1.4}$ (solid line) is compared to the linear fit (dashed line). Also shown is the evaluated position of the metal – insulator transition. (Adopted from Ref. [27].) (b) Dependence of B_c on electron density, obtained from measurements of the parallel-field magnetoresistance in highly disordered samples of narrow AlAs quantum wells. The solid curve represents the quantum Monte Carlo calculation for a disorder-free 2D electron system [5]. The dashed line portrays a linear fit. The evaluated position of the metal – insulator transition is also indicated. (Adopted from Ref. [235].)

dielectric constant and the presence of a spacer. Moreover, it is distinguished from other systems by its remote-doping scattering, as indicated by the small parallel-field magnetoresistance [236]. A similar increase in the spin susceptibility at low densities was observed in this electron system, the lowest achievable densities also being well above the expected critical region for $n_s < 4 \times 10^{10}$ cm^{-2} [237]. Thus, in all the studied dilute 2D electron systems other than silicon MOSFETs, too high disorder and, hence, too high electron densities for the metal – insulator transition (see Fig. 1) mask possible critical behavior of the spin susceptibility.

3.2 Determining separately the effective mass and g factor

3.2.1 Slope of the metallic temperature dependence of conductivity in a zero magnetic field. The great enhancement of the spin susceptibility $\chi \propto gm$ at low electron densities can be caused, in principle, by an increase in either g or m, or both. The effective mass and g factor were determined separately using the recent theory of temperature-dependent corrections to conductivity due to electron – electron interactions [238]. Note that its main advantage compared to the temperature-dependent screening theories [209 – 212] is that spin exchange effects are treated carefully in the new theory. At intermediate temperatures, the predicted dependence $\sigma(T)$ shows up as a linear function

$$\frac{\sigma(T)}{\sigma_0} = 1 - A^* k_B T, \qquad A^* = -\frac{(1 + 8F_0^a)\, gm}{\pi \hbar^2 n_s}, \tag{5}$$

where σ_0 is the value obtained by extrapolating the linear portion of the $\sigma(T)$ dependence to $T = 0$, and the numerical factor 8 is expected for temperatures lower than the valley splitting in silicon MOSFETs. The slope A^* is determined by the Fermi liquid constants F_0^a and F_1^s that define the renormalization of g and m: $g/g_0 = 1/(1 + F_0^a)$, and $m/m_b = 1 + F_1^s$. Using these relationships one obtains both g and m from the data for the slope A^* and the product gm [28].

For sufficiently small deviations $|\sigma/\sigma_0 - 1|$, the temperature dependence of the normalized conductivity σ/σ_0 at different electron densities above the critical density n_c for the metal – insulator transition is linear over a wide enough interval of temperatures (see Fig. 18a). The inverse slope $1/A^*$ and the quantity $\mu_B B_c$ are close to each other in a wide range of electron densities (see Fig. 18b). Moreover, the low-density data for $1/A^*$ are approximated well by a linear dependence which extrapolates to the critical density n_c in a way similar to the behavior of B_c. This finding immediately points to approximate constancy of the g factor at low electron densities, in accord with the functional form of the slope A^* in expression (5).

Renormalizations g/g_0 and m/m_b as functions of the electron density, determined from this analysis, corroborate earlier results produced at high densities but are striking in the limit of low electron densities (see Fig. 18c). Over the high-n_s region, the enhancement of both g and m is relatively small, both quantities increasing slightly with decreasing electron density in agreement with earlier data [239]. Also, the renormalization of the g factor is dominant compared to that of the effective mass, in agreement with theoretical studies [240 – 242]. In contrast, over the low-n_s region, the renormalization of the effective mass increases sharply with decreasing density, while the g factor remains nearly constant. Hence, it is the effective mass, rather than the g factor, that is responsible for the drastically enhanced spin susceptibility near the metal – insulator transition.

Normally, no difference is assumed between the interaction parameter $r_s^* = E_{ee}/E_F$ and the Wigner – Seitz radius $r_s = 1/(\pi n_s)^{1/2} a_B$. The finding of the greatly enhanced effective mass breaks the equivalence of r_s^* and r_s, because they are connected through the n_s-dependent mass: $r_s^* = 2(m/m_b) r_s$, where the numerical factor 2 comes from the valley degeneracy in silicon MOSFETs. Therefore, as one approaches the metal – insulator transition in low-disordered silicon MOSFETs, the interaction parameter r_s^* grows much more rapidly than r_s, reaching the values of $r_s^* > 50$ [28].

In similar experimental verifications of the theory [238] on another 2D carrier systems, much higher values of F_0^a compared to the expected limit $F_0^a = -1$ for the Stoner instability were found for the metallic slope of $\sigma(T)$ dependences [243 – 246]. The relatively small enhancement

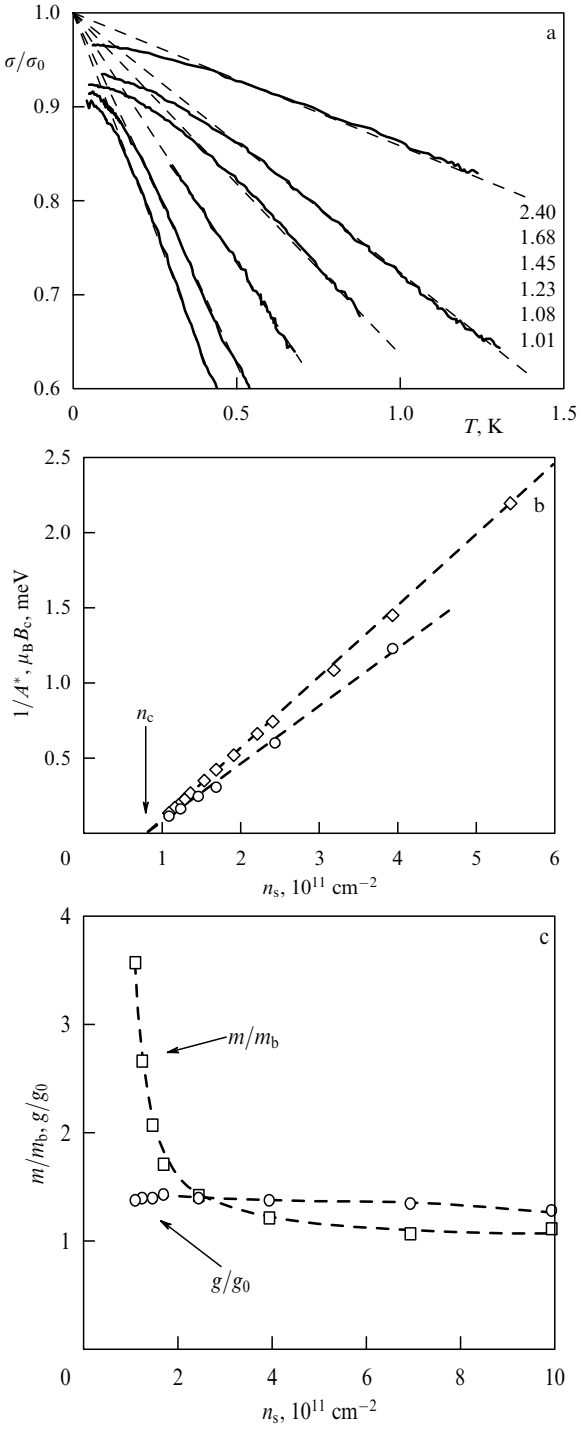

Figure 18. (a) The temperature dependence of the normalized conductivity in a low-disordered silicon MOSFET at different electron densities (indicated in units of 10^{11} cm^{-2}) above the critical electron density for the metal – insulator transition. The dashed lines depict fits to the linear portion of the dependence. (b) The inverse slope $1/A^*$ (circles) and the polarization field B_c (diamonds) as functions of electron density. The dashed lines are linear fits which extrapolate to the critical density for the metal – insulator transition. (c) The effective mass and g factor versus electron density, determined from an analysis of the temperature-dependent conductivity and parallel-field magnetoresistance. The dashed lines portray guides for the eye. (Taken from Ref. [28].)

of the g factor indicates that the spin exchange effects are not very pronounced. From an experimental point of view, this raises a problem of comparison between different theories. Formally, even if there are possible uncertainties in the coefficients entering theoretical relationships, both the temperature-dependent screening theories [209 – 212] and the theory developed in work [238] describe reasonably well the available experimental data [247, 248]. To discriminate between these two, more detailed comparison with experiment is needed. Note that the slope A^* in Eqn (5) is proportional to the effective mass in all theories, so that the conclusion about the greatly enhanced effective mass at low electron densities in low-disordered silicon MOSFETs is basically independent of a particular theory.

3.2.2 Temperature-dependent amplitude of the weak-field Shubnikov – de Haas oscillations. The claim about a sharp increase in the effective mass was verified based on the analysis of the temperature dependence of the Shubnikov – de Haas oscillations. The approach was similar to that used by Smith and Stiles [214], but it was extended to much lower electron densities and temperatures [29]. The $\rho(T)$ dependence becomes saturated in the low-temperature limit, and the Lifshitz – Kosevich formula with a constant Dingle temperature for the weak-field oscillation amplitude of the normalized resistance:

$$\frac{A(T)}{A_0} = \frac{2\pi^2 k_B T/\hbar\omega_c}{\sinh(2\pi^2 k_B T/\hbar\omega_c)}\,,$$
$$A_0 = 4\exp\left(-\frac{2\pi^2 k_B T_D}{\hbar\omega_c}\right), \qquad (6)$$

where $\omega_c = eB_\perp/mc$ is the cyclotron frequency, and T_D is the Dingle temperature, describes damping of the Shubnikov – de Haas oscillations with temperature (see Fig. 19a). The effective mass as a function of electron density, determined by this method, agrees well with the data obtained by the procedure described in the preceding section (see Fig. 19b). The agreement between the results produced using two independent methods supports the validity of both and justifies the applicability of formulas (6) to the strongly interacting 2D electron system in silicon MOSFETs.

To probe a possible contribution from the spin exchange interactions to the effective mass enhancement, a parallel magnetic field component was introduced to align the electrons' spins. Within the limits of experimental accuracy, the effective mass does not depend on the degree of spin polarization $\xi = (B_\perp^2 + B_\parallel^2)^{1/2}/B_c$ (see Fig. 19c). Therefore, the $m(n_s)$ dependence is robust, and the origin of the mass enhancement has no relation to the electrons' spins and exchange effects.

A similar analysis of the Shubnikov – de Haas oscillations in dilute silicon MOSFETs at high temperatures $T > 0.3$ K, where the low-density resistivity (and, hence, T_D) crucially depends on temperature, allows an evaluation of the effective mass as well as the g factor which is calculated from the known value of gm [224] (see Fig. 20). The two data sets are obtained based on unlike assumptions of a temperature-independent Dingle temperature and that of a Dingle temperature that increases linearly with temperature. Too large a scatter in the results makes it impossible to establish which quantity (either g or m, or both) is responsible for the great enhancement of the spin susceptibility. Note that an attempt to improve the evaluation of the effective mass by justifying the application of the Lifshitz – Kosevich formula with a temperature-dependent T_D [249] would lead, on the contrary, to bigger deviations of the estimated values of mass

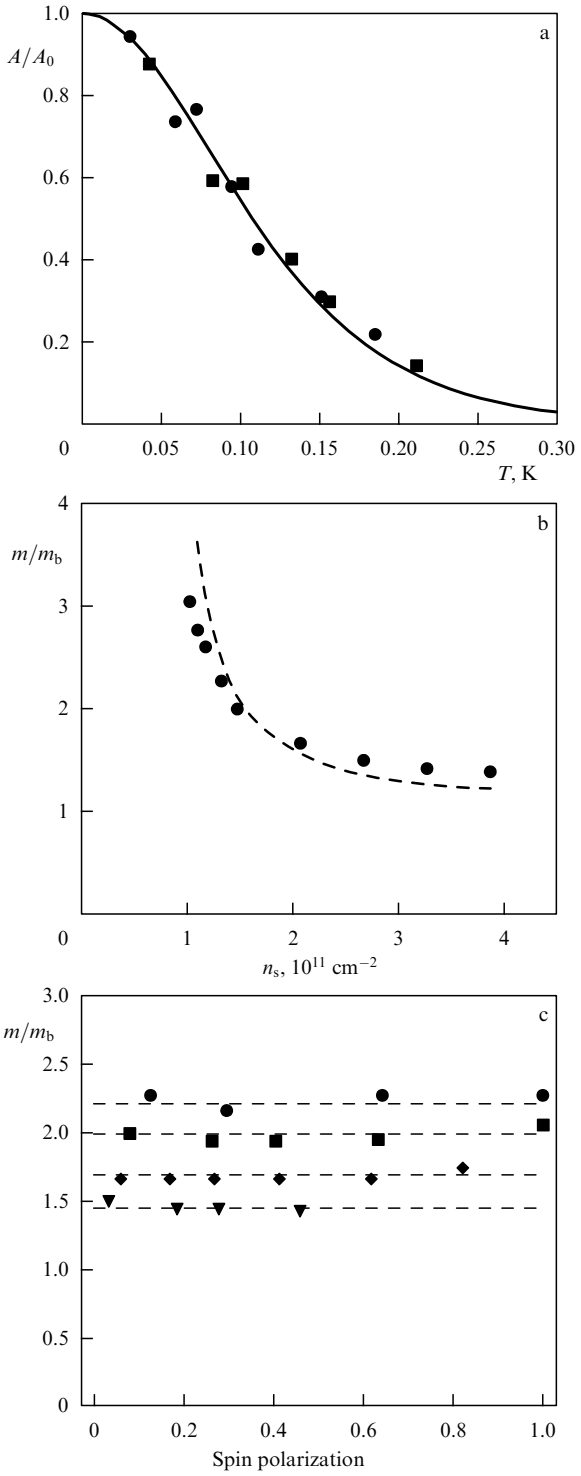

Figure 19. (a) Variation of the amplitude of the weak-field Shubnikov–de Haas oscillations in a low-disordered silicon MOSFET with temperature at $n_s = 1.17 \times 10^{11}$ cm^{-2} for oscillation numbers $\nu = 10$ (circles) and $\nu = 14$ (squares). The value of T for the $\nu = 10$ data is lowered by a factor of 1.4. The solid line depicts a fit using Eqn (6). (b) Dependence of the effective mass on electron density, determined from an analysis of Shubnikov–de Haas oscillations (circles) and from an analysis of $\sigma(T)$ and $\rho(B_{\|})$ curves (dashed line). (c) The effective mass versus the degree of spin polarization for the following electron densities (in units of 10^{11} cm^{-2}): 1.32 (circles), 1.47 (squares), 2.07 (diamonds), and 2.67 (triangles). The dashed lines present guides for the eye. (Taken from Ref. [29].)

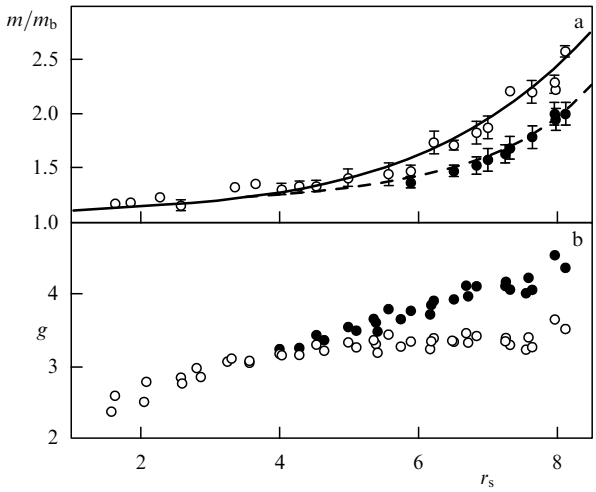

Figure 20. The effective mass and g factor in a dilute silicon MOSFET as functions of r_s. Distinct symbols correspond to two different assumptions for evaluating m from an analysis of the high-temperature Shubnikov–de Haas oscillations: a temperature-independent T_D (open circles), and a Dingle temperature that linearly increases with temperature (solid circles). The solid and dashed lines in figure (a) are polynomial fits. (Adopted from Ref. [224].)

from the results obtained in the low-temperature limit (cf. Figs 19b and 20).

An analysis of the temperature-dependent amplitude of Shubnikov–de Haas oscillations in a dilute 2D electron system in narrow AlAs quantum wells yielded moderate enhancements of the effective mass as well as the g factor determined from the known gm [235]. The observed behavior of g and m is similar to that found at high electron densities in silicon MOSFETs. This indicates that the valley origin of the greatly enhanced effective mass at low electron densities in silicon MOSFETs is not very likely, even though the lowest accessible electron densities in narrow AlAs quantum wells are still too high. Interestingly, the observed values of g/g_0 in the limit of high electron densities in AlAs quantum wells exceed appreciably the value of $g/g_0 = 1$, as well as those found in silicon MOSFETs. The increase in the spin susceptibility with the strain-induced valley polarization, observed at high electron densities in AlAs quantum wells [250], is likely to be connected with an increase in the g factor.

3.2.3 Spin and cyclotron gaps in strong magnetic fields. The results for the great enhancement of the effective mass are also consistent with the data for spin and cyclotron gaps, which were obtained by magnetocapacitance spectroscopy. The experimental procedure is based on determination of the chemical potential jumps in a 2D electron system, when the filling factor traverses the gaps in the spectrum. A dip in the magnetocapacitance at the integer filling factor is directly related to a jump of the chemical potential across a corresponding gap in the spectrum of the 2D electron system [251, 252]:

$$\frac{1}{C} = \frac{1}{C_0} + \frac{1}{A_g e^2 \, \mathrm{d}n_s/\mathrm{d}\mu} \,, \tag{7}$$

where C_0 is the geometric capacitance, and A_g is the sample area. The chemical potential jump is determined by integrating the magnetocapacitance over the dip in the low-tempera-

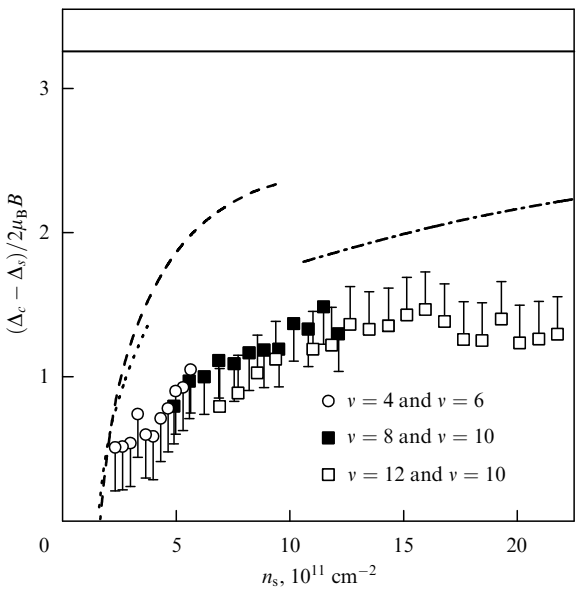

Figure 21. Difference of the normalized values of cyclotron and spin gaps in a perpendicular magnetic field versus electron density for silicon MOSFETs. The level width contribution is indicated by systematic error bars. Also shown for comparison is the value of $(m_e/m - g)$ determined from the data of Ref. [28] (dashed line), Ref. [29] (dotted line), and Ref. [214] (dot-and-dash line), as well as by using the band electron mass and the g factor in bulk silicon (solid line). (Taken from Ref. [254].)

ture limit where the magnetocapacitance saturates and becomes independent of temperature [253]. It should be emphasized that conventional measurements of the activation energy yield a mobility gap which may be different from the gap in the energy spectrum. This is a serious disadvantage as compared to the direct method of magnetocapacitance spectroscopy.

The g factor determined by this procedure is close to its value in bulk silicon and does not change with the filling factor [254], in disagreement with the theory of exchange-enhanced gaps [215–219]. The cyclotron splitting corresponds to the effective mass that is greatly enhanced at low electron densities (see Fig. 21). Thus, the spin exchange effects are still not pronounced in strong magnetic fields.

It is worth noting that in contrast to the g factor, the valley gap is greatly enhanced at the lowest filling factors $\nu = 1$ and $\nu = 3$ and oscillates with ν [253, 254]. This is similar to the behavior of the spin gap in GaAs/AlGaAs heterostructures [255, 256], both of the gaps increasing linearly with a growth of the perpendicular magnetic field.

3.3 Wigner crystal or ferromagnetic Fermi liquid, as analyzed from theoretical approaches

As has been mentioned above, the experimental results obtained in low-disordered silicon MOSFETs indicate that the metal–insulator transition is driven by electron interactions on the metallic side. In contrast, on the insulating side this is still a classical percolation transition with no dramatic interaction effects. One then concludes that the vicinity of either tricritical point in the phase diagram in Fig. 1 is reached. This is consistent with the fact that the interaction parameter r_s^* at low electron densities exceeds the theoretical estimate for the onset of Wigner crystallization, even though it is not yet clear whether or not electron crystallization expected in the low-density limit is preceded by an intermediate phase like a ferromagnetic Fermi liquid.

To address the problem, two approaches have been formulated. The first one exploits the Fermi liquid model, extending it to the region of relatively large r_s^*. Its outcome is that the renormalization of g factor is large compared to that of m [240–242]. In the limiting case of high r_s^*, one may expect a divergence of the g factor that corresponds to the Stoner instability. These predictions are in contradiction to the experimental evidence. First, the dilute system behavior in the regime of the greatly enhanced susceptibility — close to the onset of spontaneous spin polarization and Wigner crystallization — is governed by the effective mass, rather than the g factor, through the interaction parameter r_s^*. And second, the insensitivity of the effective mass enhancement to spin exchange effects cannot be accounted for. This discrepancy diminishes somewhat the chances for the occurrence of a ferromagnetic Fermi liquid that precedes electron crystallization. In principle, should the spin exchange be small, the spin effects may still come into play closer to the onset of Wigner crystallization, where the Fermi energy may continue dropping as caused by mass enhancement.

The other theoretical approach is not based on a Fermi liquid. In analogy with He^3, the existence of an intermediate phase between the Fermi liquid and the Wigner crystal, caused by a partial separation of the uniform phases, was predicted [257]. It was also foretold that the renormalization of m near the crystallization point is dominant compared to that of g and that the effective mass may diverge at the transition point and should increase with the magnetic field intensity [258]. The significant increase in the effective mass near the electron crystallization point also follows from Gutzwiller's variational method [259] which was applied to silicon MOSFETs [260], and from the dynamical mean-field theory [261]. Although the sharp increase in the mass is in agreement with the experimental results, the suggested dependence of m on the degree of spin polarization is not confirmed by the available data.

Concluding this section, I would like to make some more remarks on the Fermi-liquid-related concepts. An idea was expressed to connect the observed effective mass enhancement to possible formation of a coupled-valley state in bivalley electron systems [262, 263]. Still, it is at odds with the fact that similar results were obtained for single-valley electron systems. An assumption was made that a plateau at the Fermi energy may form in the $E(k)$ spectrum, thus leading to a diverging effective mass (see, e.g., Ref. [264]). As for now, however, the dependence of the effective mass on temperature, resulting from the plateau formation, is not consistent with the experimental findings. A prediction that the electron density, at which the effective mass exhibits a sharp increase, is sensitive to disorder [265] was not confirmed by the experimental data from available samples. After all, one can simply follow a classical way of phenomenologically introducing Fermi-liquid parameters as the physical observables to be determined in experiment.

4. Conclusions

A critical analysis of the available experimental data for 2D electron systems shows that the consequences of the scaling theory of localization are not confirmed. The main points to be addressed by the theorists are the problem of finite

bandwidth of the extended states in the Landau levels and that of a true metal–insulator transition in a zero magnetic field, whose existence is strongly supported in low-disordered 2D electron systems, but remains uncertain in 2D electron systems with high disorder. Also, there is still no theoretical description of the oscillations of the metal–insulator phase boundary as a function of a perpendicular magnetic field.

In the past four years, significant progress has been made in understanding the metallic state in strongly interacting low-disordered 2D electron systems. This state is remarkable for the strong metallic temperature dependence of the resistivity, caused by electron–electron interaction effects. The spin susceptibility measured in low-disordered silicon MOSFETs using different experimental procedures shows a sharp increase and possible divergence at a finite sample-independent electron density n_χ close to the critical density n_c for the metal–insulator transition. This indicates that the metal–insulator transition in clean 2D systems is driven by interactions. Unlike the Stoner instability, the increase in the spin susceptibility is caused by the enhanced effective mass rather than the g factor. The effective mass does not depend on the degree of spin polarization, so that the mass enhancement is not due to spin exchange. A similar increase in the spin susceptibility was observed in other 2D carrier systems. It remains to be seen whether or not this increase indicates the occurrence of a spontaneous spin polarization at a finite carrier density.

I am grateful to I L Aleiner, M W C Dharma-wardana, V T Dolgopolov, M M Fogler, V F Gantmakher, D Heiman, S V Kravchenko, D N Sheng, and A Widom for valuable discussions. The author is supported by the Russian Foundation for Basic Research and the RF Ministry for Education and Science.

References

1. Wigner E *Phys. Rev.* **46** 1002 (1934)
2. Stoner E C *Rep. Prog. Phys.* **11** 43 (1946)
3. Landau L D *Zh. Eksp. Teor. Fiz.* **32** 59 (1957) [*Sov. Phys. JETP* **5** 101 (1957)]
4. Tanatar B, Ceperley D M *Phys. Rev. B* **39** 5005 (1989)
5. Attaccalite C et al. *Phys. Rev. Lett.* **88** 256601 (2002)
6. Abrahams E et al. *Phys. Rev. Lett.* **42** 673 (1979)
7. Altshuler B L, Aronov A G, Lee P A *Phys. Rev. Lett.* **44** 1288 (1980)
8. Finkel'shtein A M *Zh. Eksp. Teor. Fiz.* **84** 168 (1983) [*Sov. Phys. JETP* **57** 97 (1983)]
9. Finkelstein A M *Z. Phys. B* **56** 189 (1984)
10. Castellani C et al. *Phys. Rev. B* **30** 527 (1984)
11. Dolan G J, Osheroff D D *Phys. Rev. Lett.* **43** 721 (1979)
12. Bishop D J, Tsui D C, Dynes R C *Phys. Rev. Lett.* **44** 1153 (1980)
13. Uren M J, Davies R A, Pepper M *J. Phys. C: Solid State Phys.* **13** L985 (1980)
14. Shashkin A A, Kravchenko G V, Dolgopolov V T *Pis'ma Zh. Eksp. Teor. Fiz.* **58** 215 (1993) [*JETP Lett.* **58** 220 (1993)]
15. Shashkin A A, Dolgopolov V T, Kravchenko G V *Phys. Rev. B* **49** 14486 (1994)
16. Shashkin A A et al. *Phys. Rev. Lett.* **73** 3141 (1994)
17. Khmelnitskii D E *Phys. Lett. A* **106** 182 (1984)
18. Laughlin R B *Phys. Rev. Lett.* **52** 2304 (1984)
19. Kravchenko S V et al. *Phys. Rev. B* **50** 8039 (1994)
20. Kravchenko S V et al. *Phys. Rev. B* **51** 7038 (1995)
21. Kravchenko S V et al. *Phys. Rev. Lett.* **77** 4938 (1996)
22. Kravchenko S V et al. *Solid State Commun.* **116** 495 (2000)
23. Shashkin A A et al. *Phys. Rev. Lett.* **87** 086801 (2001)
24. Vitkalov S A et al. *Phys. Rev. Lett.* **87** 086401 (2001)
25. Kravchenko S V, Shashkin A A, Dolgopolov V T *Phys. Rev. Lett.* **89** 219701 (2002)
26. Gao X P A et al. *Phys. Rev. Lett.* **89** 016801 (2002)
27. Zhu J et al. *Phys. Rev. Lett.* **90** 056805 (2003)
28. Shashkin A A et al. *Phys. Rev. B* **66** 073303 (2002)
29. Shashkin A A et al. *Phys. Rev. Lett.* **91** 046403 (2003)
30. Shashkin A A et al. *J. Phys. A: Math. Gen.* **36** 9237 (2003)
31. Abrahams E, Kravchenko S V, Sarachik M P *Rev. Mod. Phys.* **73** 251 (2001)
32. Kravchenko S V, Sarachik M P *Rep. Prog. Phys.* **67** 1 (2004)
33. Lozovik Yu E, Yudson V I *Pis'ma Zh. Eksp. Teor. Fiz.* **22** 26 (1975) [*JETP Lett.* **22** 11 (1975)]
34. Tsukada M *J. Phys. Soc. Jpn.* **42** 391 (1977)
35. Maki K, Zotos X *Phys. Rev. B* **28** 4349 (1983)
36. Lam P K, Girvin S M *Phys. Rev. B* **30** 473 (1984)
37. Levesque D, Weiss J J, MacDonald A H *Phys. Rev. B* **30** 1056 (1984)
38. D'Iorio M, Pudalov V M, Semenchinsky S G *Phys. Lett. A* **150** 422 (1990)
39. Kravchenko S V, Perenboom J A A J, Pudalov V M *Phys. Rev. B* **44** 13513 (1991)
40. D'Iorio M, Pudalov V M, Semenchinsky S G *Phys. Rev. B* **46** 15992 (1992)
41. Pudalov V M et al. *Phys. Rev. Lett.* **70** 1866 (1993)
42. Willett R L et al. *Phys. Rev. B* **38** 7881 (1988)
43. Goldman V J, Shayegan M, Tsui D C *Phys. Rev. Lett.* **61** 881 (1988)
44. Andrei E Y et al. *Phys. Rev. Lett.* **60** 2765 (1988)
45. Willett R L et al. *Phys. Rev. B* **40** 6432 (1989)
46. Jiang H W et al. *Phys. Rev. Lett.* **65** 633 (1990)
47. Goldman V J et al. *Phys. Rev. Lett.* **65** 2189 (1990)
48. Williams F I B et al. *Phys. Rev. Lett.* **66** 3285 (1991)
49. Jiang H W et al. *Phys. Rev. B* **44** 8107 (1991)
50. Santos M B et al. *Phys. Rev. Lett.* **68** 1188 (1992)
51. Santos M B et al. *Phys. Rev. B* **46** 13639 (1992)
52. Manoharan H C, Shayegan M *Phys. Rev. B* **50** 17662 (1994)
53. v. Klitzing K, Dorda G, Pepper M *Phys. Rev. Lett.* **45** 494 (1980)
54. Kivelson S, Lee D-H, Zhang S-C *Phys. Rev. B* **46** 2223 (1992)
55. Khmelnitskii D E *Helv. Phys. Acta* **65** 164 (1992)
56. Huckestein B *Phys. Rev. Lett.* **84** 3141 (2000)
57. Dolgopolov V T et al. *Phys. Rev. B* **46** 13303 (1992)
58. Kravchenko S V et al. *Phys. Rev. Lett.* **75** 910 (1995)
59. Dultz S C, Jiang H W, Schaff W J *Phys. Rev. B* **58** R7532 (1998)
60. Hilke M et al. *Phys. Rev. B* **62** 6940 (2000)
61. Glozman I, Johnson C E, Jiang H W *Phys. Rev. Lett.* **74** 594 (1995)
62. Shashkin A A et al. *Phys. Rev. Lett.* **75** 2248 (1995)
63. Pudalov V M, D'Iorio M, Campbell J W *Pis'ma Zh. Eksp. Teor. Fiz.* **57** 592 (1993) [*JETP Lett.* **57** 608 (1993)]
64. Jiang H W et al. *Phys. Rev. Lett.* **71** 1439 (1993)
65. Shahar D, Tsui D C, Cunningham J E *Phys. Rev. B* **52** R14372 (1995)
66. Hilke M et al. *Phys. Rev. B* **56** R15545 (1997)
67. Sakr M R et al. *Phys. Rev. B* **64** 161308 (2001)
68. Wang T et al. *Phys. Rev. Lett.* **72** 709 (1994)
69. Hughes R J F et al. *J. Phys.: Condens. Matter* **6** 4763 (1994)
70. Song S-H et al. *Phys. Rev. Lett.* **78** 2200 (1997)
71. Lee C H et al. *Phys. Rev. B* **58** 10629 (1998)
72. Hilke M et al. *Nature* **395** 675 (1998)
73. Hilke M et al. *Europhys. Lett.* **46** 775 (1999)
74. Hanein Y et al. *Nature* **400** 735 (1999)
75. Popović D, Fowler A B, Washburn S *Phys. Rev. Lett.* **79** 1543 (1997)
76. Coleridge P T et al. *Phys. Rev. B* **56** R12764 (1997)
77. Shashkin A A, Kravchenko S V, Klapwijk T M *Phys. Rev. Lett.* **87** 266402 (2001)
78. Papadakis S J, Shayegan M *Phys. Rev. B* **57** R15068 (1998)
79. Hanein Y et al. *Phys. Rev. Lett.* **80** 1288 (1998)
80. Simmons M Y et al. *Phys. Rev. Lett.* **80** 1292 (1998)
81. Mills A P (Jr) et al. *Phys. Rev. Lett.* **83** 2805 (1999)
82. Yoon J et al. *Phys. Rev. Lett.* **82** 1744 (1999)
83. Simmons M Y et al. *Phys. Rev. Lett.* **84** 2489 (2000)
84. Noh H et al. *Phys. Rev. B* **68** 165308 (2003)
85. Pudalov V M et al., cond-mat/0103087
86. Fogler M M, Shklovskii B I *Phys. Rev. B* **52** 17366 (1995)
87. Tikofsky A M, Kivelson S A *Phys. Rev. B* **53** R13275 (1996)
88. Ando T *J. Phys. Soc. Jpn.* **53** 3126 (1984)
89. Shahbazyan T V, Raikh M E *Phys. Rev. Lett.* **75** 304 (1995)
90. Kagalovsky V, Horovitz B, Avishai Y *Phys. Rev. B* **52** R17044 (1995)

91. Gramada A, Raikh M E *Phys. Rev. B* **54** 1928 (1996)
92. Haldane F D M, Yang K *Phys. Rev. Lett.* **78** 298 (1997)
93. Fogler M M *Phys. Rev. B* **57** 11947 (1998)
94. Liu D Z, Xie X C, Niu Q *Phys. Rev. Lett.* **76** 975 (1996)
95. Xie X C et al. *Phys. Rev. B* **54** 4966 (1996)
96. Hatsugai Y, Ishibashi K, Morita Y *Phys. Rev. Lett.* **83** 2246 (1999)
97. Yang K, Bhatt R N *Phys. Rev. Lett.* **76** 1316 (1996)
98. Yang K, Bhatt R N *Phys. Rev. B* **59** 8144 (1999)
99. Koschny Th, Potempa H, Schweitzer L *Phys. Rev. Lett.* **86** 3863 (2001)
100. Pereira A L C, Schulz P A *Phys. Rev. B* **66** 155323 (2002)
101. Koschny Th, Schweitzer L *Phys. Rev. B* **67** 195307 (2003)
102. Sheng D N, Weng Z Y *Phys. Rev. Lett.* **78** 318 (1997)
103. Sheng D N, Weng Z Y *Phys. Rev. B* **62** 15363 (2000)
104. Okamoto T, Shinohara Y, Kawaji S *Phys. Rev. B* **52** 11109 (1995)
105. Dultz S C, Jiang H W *Phys. Rev. Lett.* **84** 4689 (2000)
106. Fogler M M *Phys. Rev. B* **69** 121409(R) (2004)
107. Dolgopolov V T, Kravchenko G V, Shashkin A A *Pis'ma Zh. Eksp. Teor. Fiz.* **55** 146 (1992) [*JETP Lett.* **55** 140 (1992)]
108. Dolgopolov V T et al. *Pis'ma Zh. Eksp. Teor. Fiz.* **55** 701 (1992) [*JETP Lett.* **55** 733 (1992)]
109. Dolgopolov V T et al. *Pis'ma Zh. Eksp. Teor. Fiz.* **62** 152 (1995) [*JETP Lett.* **62** 168 (1995)]
110. Adkins C J, Pollitt S, Pepper M *J. Phys. Colloq.* (Paris) **37** (C4) 343 (1976)
111. Polyakov D G, Shklovskii B I *Phys. Rev. B* **48** 11167 (1993)
112. Shklovskii B I, Efros A L *Electronic Properties of Doped Semiconductors* (New York: Springer-Verlag, 1984)
113. Li Y P, PhD Thesis (Princeton, NJ: Princeton Univ., 1994)
114. Kukushkin I V, Timofeev V B *Usp. Fiz. Nauk* **163** (7) 1 (1993) [*Sov. Phys. Usp.* **36** 549 (1993)]
115. Iordansky S V *Solid State Commun.* **43** 1 (1982)
116. Ando T *J. Phys. Soc. Jpn.* **52** 1740 (1983)
117. Aoki H *J. Phys. C*: *Solid State Phys.* **16** 1893 (1983)
118. Aoki H, Ando T *Phys. Rev. Lett.* **54** 831 (1985)
119. Pruisken A M M *Phys. Rev. Lett.* **61** 1297 (1988)
120. Wei H P et al. *Phys. Rev. Lett.* **61** 1294 (1988)
121. Wakabayashi J, Yamane M, Kawaji S *J. Phys. Soc. Jpn.* **58** 1903 (1989)
122. Koch S et al. *Phys. Rev. B* **43** 6828 (1991)
123. Dolgopolov V T et al. *Zh. Eksp. Teor. Fiz.* **99** 201 (1991) [*Sov. Phys. JETP* **72** 113 (1991)]
124. Koch S et al. *Phys. Rev. Lett.* **67** 883 (1991)
125. Koch S et al. *Phys. Rev. B* **46** 1596 (1992)
126. Wei H P et al. *Phys. Rev. B* **45** 3926 (1992)
127. Hwang S W et al. *Phys. Rev. B* **48** 11416 (1993)
128. Engel L W et al. *Phys. Rev. Lett.* **71** 2638 (1993)
129. Wei H P, Engel L W, Tsui D C *Phys. Rev. B* **50** 14609 (1994)
130. Wong L W et al. *Phys. Rev. B* **51** 18033 (1995)
131. Shahar D et al. *Phys. Rev. Lett.* **74** 4511 (1995)
132. Pan W et al. *Phys. Rev. B* **55** 15431 (1997)
133. Shahar D et al. *Phys. Rev. Lett.* **79** 479 (1997)
134. Coleridge P T *Phys. Rev. B* **60** 4493 (1999)
135. van Schaijk R T F et al. *Phys. Rev. Lett.* **84** 1567 (2000)
136. Dunford R B et al. *Physica E* **6** 297 (2000)
137. Dunford R B et al. *Physica B* **298** 496 (2001)
138. Hohls F, Zeitler U, Haug R J *Phys. Rev. Lett.* **86** 5124 (2001)
139. Hohls F, Zeitler U, Haug R J *Phys. Rev. Lett.* **88** 036802 (2002)
140. Hohls F et al. *Phys. Rev. Lett.* **89** 276801 (2002)
141. Balaban N Q, Meirav U, Bar-Joseph I *Phys. Rev. Lett.* **81** 4967 (1998)
142. Shahar D et al. *Solid State Commun.* **107** 19 (1998)
143. Arapov Y G et al. *Nanotechnology* **13** 86 (2002)
144. Huckestein B *Rev. Mod. Phys.* **67** 357 (1995)
145. Wysokinski K I, Brenig W *Z. Phys. B* **54** 11 (1983)
146. Viehweger O, Efetov K B *J. Phys.*: *Condens. Matter* **2** 7049 (1990)
147. Viehweger O, Efetov K B *Phys. Rev. B* **44** 1168 (1991)
148. Zhang S-C, Kivelson S, Lee D-H *Phys. Rev. Lett.* **69** 1252 (1992)
149. Wakabayashi J et al. *J. Phys. Soc. Jpn.* **57** 3678 (1988)
150. Dorozhkin S I et al. *Pis'ma Zh. Eksp. Teor. Fiz.* **57** 55 (1993) [*JETP Lett.* **57** 58 (1993)]
151. Goldman V J et al. *Phys. Rev. Lett.* **70** 647 (1993)
152. Sajoto T et al. *Phys. Rev. Lett.* **70** 2321 (1993)
153. Kravchenko S V, Furneaux J E, Pudalov V M *Phys. Rev. B* **49** 2250 (1994)
154. Pudalov V M, D'Iorio M, Campbell J W *Surf. Sci.* **305** 107 (1994)
155. Levine H, Libby S B, Pruisken A M M *Phys. Rev. Lett.* **51** 1915 (1983)
156. Khmel'nitskiĭ D E *Pis'ma Zh. Eksp. Teor. Fiz.* **38** 454 (1983) [*JETP Lett.* **38** 552 (1983)
157. Dykhne A M, Ruzin I M *Phys. Rev. B* **50** 2369 (1994)
158. Ruzin I, Feng S *Phys. Rev. Lett.* **74** 154 (1995)
159. Burgess C P, Dib R, Dolan B P *Phys. Rev. B* **62** 15359 (2000)
160. Wei H P, Tsui D C, Pruisken A M M *Phys. Rev. B* **33** 1488 (1986)
161. Halperin B I *Phys. Rev. B* **25** 2185 (1982)
162. Prange R E, Girvin S M (Eds) *The Quantum Hall Effect* (New York: Springer-Verlag, 1987)
163. Büttiker M *Phys. Rev. B* **38** 9375 (1988)
164. Laughlin R B *Phys. Rev. B* **23** 5632 (1981)
165. Widom A, Clark T D *J. Phys. D*: *Appl. Phys.* **15** L181 (1982)
166. Dolgopolov V T, Zhitenev N B, Shashkin A A *Pis'ma Zh. Eksp. Teor. Fiz.* **52** 826 (1990) [*JETP Lett.* **52** 196 (1990)]
167. Dolgopolov V T, Zhitenev N B, Shashkin A A *Europhys. Lett.* **14** 255 (1991)
168. Dolgopolov V T et al. *Phys. Rev. B* **46** 12560 (1992)
169. Dolgopolov V T et al. *Phys. Rev. B* **48** 8480 (1993)
170. Jeanneret B et al. *Phys. Rev. B* **51** 9752 (1995)
171. Watts J P et al. *Phys. Rev. Lett.* **81** 4220 (1998)
172. Honold M M et al. *Phys. Rev. B* **59** R10417 (1999)
173. Dolgopolov V T et al. *Phys. Rev. Lett.* **86** 5566 (2001)
174. Dolgopolov V T, Kravchenko G V, Shashkin A A *Solid State Commun.* **78** 999 (1991)
175. Haug R J *Semicond. Sci. Technol.* **8** 131 (1993)
176. Fontein P F et al. *Phys. Rev. B* **43** 12090 (1991)
177. Kent A J et al. *Phys. Rev. Lett.* **69** 1684 (1992)
178. Merz R et al. *Phys. Rev. Lett.* **70** 651 (1993)
179. Shashkin A A et al. *Semicond. Sci. Technol.* **9** 2110 (1994)
180. Shashkin A A et al. *Phys. Rev. B* **49** 5379 (1994)
181. van Haren R J F, Blom F A P, Wolter J H *Phys. Rev. Lett.* **74** 1198 (1995)
182. van Haren R J F et al. *Phys. Rev. B* **52** 5760 (1995)
183. Shashkin A A et al. *Phys. Rev. Lett.* **79** 5114 (1997)
184. Wei Y Y et al. *Phys. Rev. Lett.* **81** 1674 (1998)
185. Tessmer S H et al. *Nature* **392** 51 (1998)
186. McCormick K L et al. *Phys. Rev. B* **59** 4654 (1999)
187. Yacoby A et al. *Solid State Commun.* **111** 1 (1999)
188. Shashkin A A et al. *Phys. Rev. B* **60** R16307 (1999)
189. Zhitenev N B et al. *Nature* **404** 473 (2000)
190. Finkelstein G et al. *Science* **289** 90 (2000)
191. Finkelstein G et al. *Phys. Rev. B* **61** R16323 (2000)
192. Woodside M T et al. *Phys. Rev. B* **64** 041310 (2001)
193. van Zalinge H et al. *Phys. Rev. B* **64** 235303 (2001)
194. Glicofridis P I et al. *Phys. Rev. B* **65** 121312(R) (2002)
195. Chklovskii D B, Shklovskii B I, Glazman L I *Phys. Rev. B* **46** 4026 (1992)
196. Ebert G, von Klitzing K, Weimann G *J. Phys. C*: *Solid State Phys.* **18** L257 (1985)
197. Pudalov V M, Semenchinskiĭ S G *Pis'ma Zh. Eksp. Teor. Fiz.* **42** 188 (1985) [*JETP Lett.* **42** 232 (1985)]
198. Shashkin A A, Dolgopolov V T, Dorozhkin S I *Zh. Eksp. Teor. Fiz.* **91** 1897 (1986) [*Sov. Phys. JETP* **64** 1124 (1986)]
199. Wiegers S A J et al. *Phys. Rev. B* **59** 7323 (1999)
200. Sarachik M P, Kravchenko S V *Proc. Natl. Acad. Sci. USA* **96** 5900 (1999)
201. Kravchenko S V, Klapwijk T M *Phys. Rev. Lett.* **84** 2909 (2000)
202. Jaroszyński J, Popović D, Klapwijk T M *Phys. Rev. Lett.* **89** 276401 (2002)
203. Simonian D, Kravchenko S V, Sarachik M P *Phys. Rev. B* **55** R13421 (1997)
204. Okamoto T et al. *Phys. Rev. Lett.* **82** 3875 (1999)
205. Vitkalov S A et al. *Phys. Rev. Lett.* **85** 2164 (2000)
206. Vitkalov S A, Sarachik M P, Klapwijk T M *Phys. Rev. B* **64** 073101 (2001)
207. Bogdanovich S, Popović D *Phys. Rev. Lett.* **88** 236401 (2002)
208. Leturcq R et al. *Phys. Rev. Lett.* **90** 076402 (2003)
209. Stern F *Phys. Rev. Lett.* **44** 1469 (1980)

210. Gold A, Dolgopolov V T *Phys. Rev. B* **33** 1076 (1986)
211. Das Sarma S *Phys. Rev. B* **33** 5401 (1986)
212. Das Sarma S, Hwang E H *Phys. Rev. Lett.* **83** 164 (1999)
213. Fang F F, Stiles P J *Phys. Rev.* **174** 823 (1968)
214. Smith J L, Stiles P J *Phys. Rev. Lett.* **29** 102 (1972)
215. Ando T, Uemura Y *J. Phys. Soc. Jpn.* **37** 1044 (1974)
216. Bychkov Yu A, Iordanskiĭ S V, Eliashberg G M *Pis'ma Zh. Eksp. Teor. Fiz.* **33** 152 (1981) [*JETP Lett.* **33** 143 (1981)]
217. Kallin C, Halperin B I *Phys. Rev. B* **30** 5655 (1984)
218. MacDonald A H, Oji H C A, Liu K L *Phys. Rev. B* **34** 2681 (1986)
219. Smith A P, MacDonald A H, Gumbs G *Phys. Rev. B* **45** 8829 (1992)
220. Simonian D et al. *Phys. Rev. Lett.* **79** 2304 (1997)
221. Pudalov V M et al. *Pis'ma Zh. Eksp. Teor. Fiz.* **65** 887 (1997) [*JETP Lett.* **65** 932 (1997)]
222. Pudalov V M et al. *Phys. Rev. Lett.* **88** 076401 (2002)
223. Dolgopolov V T, Gold A *Pis'ma Zh. Eksp. Teor. Fiz.* **71** 42 (2000) [*JETP Lett.* **71** 27 (2000)]
224. Pudalov V M et al. *Phys. Rev. Lett.* **88** 196404 (2002)
225. Vitkalov S A, Sarachik M P, Klapwijk T M *Phys. Rev. B* **65** 201106(R) (2002)
226. Sarachik M P, Vitkalov S A *J. Phys. Soc. Jpn. Suppl. A* **72** 53 (2003)
227. Prus O et al. *Phys. Rev. B* **67** 205407 (2003)
228. Dolgopolov V T, Gold A *Phys. Rev. Lett.* **89** 129701 (2002)
229. Gold A, Dolgopolov V T *J. Phys.: Condens. Matter* **14** 7091 (2002)
230. Batke E, Tu C W *Phys. Rev. B* **34** 3027 (1986)
231. Das Sarma S, Hwang E H *Phys. Rev. Lett.* **84** 5596 (2000)
232. Tutuc E, Melinte S, Shayegan M *Phys. Rev. Lett.* **88** 036805 (2002)
233. Noh H et al. *Phys. Rev. B* **68** 165308 (2003)
234. Tutuc E et al. *Phys. Rev. B* **67** 241309(R) (2003)
235. Vakili K et al. *Phys. Rev. Lett.* **92** 226401 (2004)
236. Dolgopolov V T et al. *Superlattices Microstruct.* **33** 271 (2003)
237. Okamoto T et al. *Phys. Rev. B* **69** 041202(R) (2004)
238. Zala G, Narozhny B N, Aleiner I L *Phys. Rev. B* **64** 214204 (2001)
239. Ando T, Fowler A B, Stern F *Rev. Mod. Phys.* **54** 437 (1982)
240. Iwamoto N *Phys. Rev. B* **43** 2174 (1991)
241. Kwon Y, Ceperley D M, Martin R M *Phys. Rev. B* **50** 1684 (1994)
242. Chen G-H, Raikh M E *Phys. Rev. B* **60** 4826 (1999)
243. Proskuryakov Y Y et al. *Phys. Rev. Lett.* **89** 076406 (2002)
244. Coleridge P T, Sachrajda A S, Zawadzki P *Phys. Rev. B* **65** 125328 (2002)
245. Vitkalov S A et al. *Phys. Rev. B* **67** 113310 (2003)
246. Pudalov V M et al. *Phys. Rev. Lett.* **91** 126403 (2003)
247. Das Sarma S, Hwang E H *Phys. Rev. Lett.* **93** 269703 (2004)
248. Shashkin A A, Dolgopolov V T, Kravchenko S V *Phys. Rev. Lett.* **93** 269705 (2004)
249. Martin G W, Maslov D L, Reizer M Yu *Phys. Rev. B* **68** 241309(R) (2003)
250. Shkolnikov Y P et al. *Phys. Rev. Lett.* **92** 246804 (2004)
251. Smith T P et al. *Phys. Rev. B* **32** 2696 (1985)
252. Pudalov V M, Semenchinskiĭ S G *Pis'ma Zh. Eksp. Teor. Fiz.* **44** 526 (1986) [*JETP Lett.* **44** 677 (1986)]
253. Khrapai V S, Shashkin A A, Dolgopolov V T *Phys. Rev. B* **67** 113305 (2003)
254. Khrapai V S, Shashkin A A, Dolgopolov V T *Phys. Rev. Lett.* **91** 126404 (2003)
255. Usher A et al. *Phys. Rev. B* **41** 1129 (1990)
256. Dolgopolov V T et al. *Phys. Rev. Lett.* **79** 729 (1997)
257. Spivak B *Phys. Rev. B* **67** 125205 (2003)
258. Spivak B *Phys. Rev. B* **64** 085317 (2001)
259. Brinkman W F, Rice T M *Phys. Rev. B* **2** 4302 (1970)
260. Dolgopolov V T *Pis'ma Zh. Eksp. Teor. Fiz.* **76** 437 (2002) [*JETP Lett.* **76** 377 (2002)]
261. Tanasković D et al. *Phys. Rev. Lett.* **91** 066603 (2003)
262. Dharma-wardana M W C *Europhys. Lett.* **67** 552 (2004)
263. Dharma-wardana M W C, Perrot F *Phys. Rev. B* **70** 035308 (2004)
264. Khodel' V A, Shaginyan V R *Pis'ma Zh. Eksp. Teor. Fiz.* **51** 488 (1990) [*JETP Lett.* **51** 553 (1990)]
265. Asgari R, Davoudi B, Tanatar B *Solid State Commun.* **130** 13 (2004)